Scientia Iranica B (2013) 20(4), 1278–1301

Sharif University of Technology
Scientia Iranica
Transactions B: Mechanical Engineering
www.scientiairanica.com

Research Note

Numerical solution of general boundary layer problems by the method of differential quadrature

S.A. Eftekhari* **and A.A. Jafari**

Department of Mechanical Engineering, K.N. Toosi University, Tehran, P.O. Box 19395-1999, Iran.

Received 4 August 2011; received in revised form 18 August 2012; accepted 23 March 2013

KEYWORDS
Differential Quadrature Method (DQM);
Blasius flow;
Sakiadis flow;
Falkner-Skan flow;
MHD Falkner-Skan flow;
Jeffery-Hamel flow;
Unsteady two-dimensional flow;
Unsteady three-dimensional MHD flow.

Abstract. Accurate numerical solutions to some boundary layer equations are presented for boundary layer flows of incompressible Newtonian fluid over a semi-infinite plate. The Differential Quadrature Method (DQM) is first used to reduce the governing nonlinear differential equations to a set of nonlinear algebraic equations. The Newton-Raphson method is then employed to solve the resulting system of nonlinear algebraic equations. The proposed formulation is applied here to solve some boundary layer problems, including Blasius, Sakiadis, Falkner-Skan, magnetohydrodynamic (MHD) Falkner-Skan, Jeffery-Hamel, unsteady two-dimensional and three-dimensional MHD flows. A simple scheme is also presented for solving the Blasius boundary layer equation. In this technique, the Blasius boundary value problem is first converted to a pair of nonlinear initial-value problems and then solved by a step-by-step DQM. The accuracy and efficiency of the proposed formulations are demonstrated by comparing the calculated results with those of other numerical and semi-analytical methods. Accurate numerical solutions are achieved using both formulations via a small number of grid points for all the cases considered.

1. Introduction

Laminar boundary layers have long been the subject of numerous studies, since they play an important role in understanding the main physical features of boundary-layer phenomena. Generally, no closed-form solutions are available for laminar boundary value problems. Therefore, many researchers have resorted to various numerical or semi-analytical methods to solve such problems. However, it is not an easy task to solve, numerically, such types of problem. The main issue is how to model such problems (with infinite or semi-infinite domains) by a method of approximation with finite grid spacing. To tackle this issue in mathematical modeling of the problem, one can apply the infinite boundary condition at a finite boundary placed at a large distance from the object (i.e., truncated boundary). This, however, begs the question of what is a 'large distance' and, obviously, substantial errors may arise if the boundary is not placed far enough away. On the other hand, pushing this out excessively far necessitates the introduction of a large number of grids to model regions of relatively little interest to the analyst. Obviously, when a low-order numerical method is used for the solution of boundary layer problems, many calculations should be done to accurately predict the location of the truncated boundary. Therefore, to accurately predict the location of the truncated boundary and to reduce the computational time, higher-order numerical methods should be used to model the boundary layer problems.

The Blasius boundary layer is an example of two-dimensional boundary layer problems. The Blasius

*. *Corresponding author. Tel.: +98-0919-4618599; Fax: +98 21 88674748.*
E-mail address: aboozar.eftekhari@gmail.com (S.A. Eftekhari)

problem models the behavior of a two-dimensional steady state laminar viscous flow of an incompressible fluid over a semi-infinite flat plate. The governing differential equation of the problem is (see [1] and Appendix A.1):

$$f'''(\eta) + \frac{1}{2} f(\eta) f''(\eta) = 0, \qquad 0 \leq \eta \leq \infty, \tag{1}$$

where η and $f(\eta)$ are the dimensionless coordinate and stream function, respectively. The boundary conditions for Eq. (1) are:

$$f(0) = f'(0) = 0, \qquad f'(\infty) = 1. \tag{2}$$

The problem was first solved by Blasius using a series expansions method. But the proposed semi-analytic series solution does not converge at all. In fact, the obtained semi-analytic solution is valid only for small values of η (i.e., the series solution converges only within a finite interval $[0, \eta_0]$, where η_0 is an unknown constant which can be determined numerically or analytically). Howarth [2] solved the Blasius equation numerically and found $\eta_0 \approx 1.8894/0.33206$. Furthermore, Asaithambi [3] solved the Blasius equation more accurately and obtained this number as $\eta_0 \approx 1.8894/0.332057336$. Due to the limitation of the Blasius power series solution, many attempts have been made to obtain solutions which are valid on the whole domain of the problem. Some researchers have solved the problem numerically and some semi-analytically. Applying the Homotopy Analysis Method (HAM) [4], Liao obtained an analytic solution for the Blasius equation which is valid in the whole region of the problem [5,6]. Using the Variational Iteration Method (VIM) [7], He constructed a five-term approximate-analytic solution for the Blasius equation which is also valid for large values of η [8]. However, the solutions obtained were not very accurate. The Adomian Decomposition Method (ADM) has also been used by some researchers to find semi-analytic solutions for the Blasius equation [9-11]. A homotopy perturbation solution to this problem was presented by He [12,13]. Kou [14], Fang et al. [15], Cortell [16], Ahmad [17], Parand and Taghavi [18], Ahmad and Al-Barakati [19] and Parand et al. [20] also solved the Blasius problem using various numerical and semi-analytical methods.

The Blasius boundary layer equation may be viewed as a special case of the Falkner-Skan equation, which has the form (see Appendix A.2):

$$f'''(\eta) + \beta_0 f(\eta) f''(\eta) + \beta \left(1 - f'(\eta)^2\right) = 0,$$

$$0 \leq \eta \leq \infty, \tag{3}$$

where β is constant. The Falkner-Skan equation arises in the study of laminar boundary layers exhibiting similarity. The solutions of the one-dimensional third-order boundary-value problem described by the well-known Falkner-Skan equation are the similarity solutions of two-dimensional incompressible laminar boundary layer equations [3]. Physically, the Falkner-Skan equation describes two-dimensional flow over stationary impenetrable wedge surfaces of included angle $\beta\pi$, which limits to a flat plate, and the Blasius solution, as β approaches zero. The solutions of the Falkner-Skan equation corresponding to $\beta > 0$ have become known as accelerating flows, those corresponding to $\beta = 0$ are called constant flows, and those corresponding to $\beta < 0$ are known as decelerating flows with separation. Physically relevant solutions exist only for $-0.19884 < \beta \leq 2$. The closed form solution for the behavior of the nonlinear two-point Falkner-Skan boundary value problem does not exist, so, such a problem has been studied by approximate numerical and semi-analytical methods, such as the shooting method [21-23], the spline collocation procedure [24], the finite difference method [25,26], the finite element method with linear interpolation functions [27], ADM [28,29], HAM [30,31], the coupling quasilinearization method and the spline method [32], the Fourier series method [33] and the collocation method [34].

When the Falkner-Skan boundary layer flow is subjected to a magnetic field, the governing differential equation for the boundary layer can be expressed as (see [35] and Appendix A.3):

$$f'''(\eta) + f(\eta) f''(\eta) + \beta(1 - f'(\eta)^2) - M^2(f'(\eta) - 1) = 0,$$

$$0 \leq \eta \leq \infty, \tag{4}$$

with the same boundary conditions as the Blasius equation (see Eq. (2)), where β and M are constants. The study of flows of this type is known as Magnetohydrodynamics or MHD for short. Such flows are of strong interest in the design and analysis of power generators, pumps, accelerators, electrostatic filters, droplet filters, heat exchangers, reactors and the like. MHD boundary layer flows have been studied by several researchers. Yih [36] and Ishak et al. [37] transformed the partial differential boundary layer equations into non-similar boundary layer equations and a system of ordinary differential equations, respectively, and then used the Keller box method to solve them. Abbasbandy and Hayat [35,38] solved MHD boundary layer flow by modified HAM and Hankel-Padé methods, respectively. Most recently, Parand et al. [39] found a solution for the problem by the pseudospectral method.

On the other hand, different from Blasius, Falkner and Skan, Sakiadis [40] considered the boundary layer flow on a moving (or stretching) flat surface in a quiescent ambient fluid. He found the same Ordinary Differential Equation (ODE) as Blasius, but the boundary conditions were different. The boundary conditions

for the Sakiadis flat-plate flow problem are (see [40] and Appendix A.4):

$$f(0) = f'(\infty) = 0, \qquad f'(0) = 1. \tag{5}$$

Tsou et al. [41] made an experimental and theoretical treatment of this problem to prove that such a flow is physically realizable. Based on the fact that a single ODE governs both Blasius and Sakiadis flow, some researchers discussed both two classical boundary-layer flows simultaneously in a single paper and provided an interesting comparison of the problems [42-44]. One of their conclusions was that the skin friction ($f''0 = \alpha$) is about 34% higher for the Sakiadis flow compared to the Blasius case. Later, Bataller [45] solved the Blasius and Sakiadis equations more accurately and obtained this value as 33.63%. Different effects, such as suction/blowing, and radiation, etc., on the above mentioned classes of flow are discussed in most recent papers by Ishak et al. [46], Fang [47] and Cortell [48]. Moreover, recent research into boundary layer flow and heat/mass transfer on a moving flat plate in a parallel stream has also been carried out by Cortell [49] and Ishak et al. [50].

As pointed out by Sakiadis [40], the non-dimensional governing differential equations for boundary layer flows on moving plates are exactly the same as those on fixed plates. Following this idea, one can easily formulate and solve the Falkner-Skan boundary layer flow and MHD Falkner-Skan boundary layer flow on moving or stretching plates. It can be easily verified that the boundary conditions for Falkner-Skan flow and MHD Falkner-Skan flow on moving or stretching plates are the same as those given in Eq. (5). With this in mind, Elgazery [28], Liao [51,52], Rashidi [53], Bognár [54] and Fathizadeh et al. [55] solved the Falkner-Skan boundary layer problem or MHD Falkner-Skan boundary layer problem using various approximate (or semi-analytic) methods.

In all the above-mentioned studies, steady two dimensional boundary layer flows were considered. Compared to the large amount of research study into two dimensional boundary layer flows, the published work on three dimensional boundary layer flows is limited. Only few works based on the steady boundary layer theory have been carried out [56-58]. The governing non-dimensional differential equations for an unsteady two dimensional boundary layer developed by an impulsively stretching plate in a constant pressure viscous flow is (see [59] and Appendix A.5):

$$f_{,\eta\eta\eta} + \frac{1}{2}(1-\xi)\eta f_{,\eta\eta} + \xi[f f_{,\eta\eta} - f_{,\eta}^2] = \xi(1-\xi) f_{,\eta\xi},$$

$$0 \le \eta \le \infty, \qquad \xi \ge 0, \tag{6}$$

subject to the boundary conditions:

$$f(0,\xi) = f_{,\eta}(\infty,\xi) = 0, \qquad f_{,\eta}(0,\xi) = 1, \tag{7}$$

where a subscript comma denotes differentiation. Liao [59] solved the above problem using the perturbation method and HAM. The unsteady three-dimensional MHD boundary layer flow and heat transfer due to an impulsively stretched plane surface were studied using HAM by Xu et al. [60] and Kumari and Nath [61]. The boundary layer equations, based on the conservation of mass, momentum and energy, governing unsteady three-dimensional flow and heat transfer on a stretching surface in the presence of a magnetic field, can be expressed in dimensionless form as (see [60,61] and Appendix A.6):

$$f_{,\eta\eta\eta} + \frac{1}{2}(1-\xi)\eta f_{,\eta\eta} + \xi[(f+s) f_{,\eta\eta} - f_{,\eta}^2 - M f_{,\eta}] = \xi(1-\xi) f_{,\eta\xi},$$

$$0 \le \eta \le \infty, \qquad \xi \ge 0, \tag{8}$$

$$s_{,\eta\eta\eta} + \frac{1}{2}(1-\xi)\eta s_{,\eta\eta} + \xi[(f+s) s_{,\eta\eta} - s_{,\eta}^2 - M s_{,\eta}] = \xi(1-\xi) s_{,\eta\xi}, \tag{9}$$

$$g_{,\eta\eta} + \frac{1}{2}\mathrm{Pr}(1-\xi)\eta g_{,\eta} + \mathrm{Pr}\xi(f+s) g_{,\eta} = \mathrm{Pr}\xi(1-\xi) g_{,\xi}, \tag{10}$$

subject to the boundary conditions:

$$f(0,\xi) = s(0,\xi) = g(\infty,\xi) = f_{,\eta}(\infty,\xi) = s_{,\eta}(\infty,\xi) = 0,$$

$$g(0,\xi) = f_{,\eta}(0,\xi) = 1, \qquad s_{,\eta}(0,\xi) = c, \tag{11}$$

where c is a positive constant, M is the magnetic parameter and Pr is the Prandtl number.

On the other hand, different from Blasius, Falkner, Skan and Sakiadis, Jeffery and Hamel [62,63] introduced the problem of the fluid flow through convergent-divergent channels. This problem has many applications in aero-space, chemical, civil, environmental, mechanical and bio-mechanical engineering, as well as in understanding rivers and canals. Jeffery-Hamel flows are interesting models of the phenomenon of the separation of boundary layers in divergent channels. These flows have revealed a multiplicity of solutions, richer perhaps than other similarity solutions of the Navier-Stokes equations, because of the dependence on two non-dimensional parameters i.e. the flow Reynolds number and channel angular widths [64]. The governing non-dimensional differential equation for the Jeffery-Hamel flow is (see Appendix A.7):

$$f'''(\eta) + 2\alpha \mathrm{Re} f(\eta) f'(\eta) + (4 - \mathrm{Ha})\alpha^2 f'(\eta) = 0,$$

$$0 \le \eta \le 1, \tag{12}$$

subject to the boundary conditions:

$$f(0) = 1, \qquad f'(0) = 0, \qquad f(1) = 0, \tag{13}$$

where Re is the Reynolds number, Ha is the Hartmann number and α is the angle of channel [64]. Closed form solutions for Jeffery-Hamel flow cannot be found in the literature, so, such boundary layer problems have to be mainly studied by approximate (or semi-analytic) methods, such as the Hermite-Padé approximation method [64], ADM [65,66], He's semi-analytical methods [67], HAM [68,69], the Optimal Homotopy Asymptotic Method (OHAM) [70], HAM, the Homotopy Perturbation Method (HPM) and the Differential Transformation Method (DTM) [71].

From a review of existing literature [1-71], it is found that most researchers are interested in the analysis of boundary layer problems using semi-analytical methods (although in some papers, the researchers call their approximate method an analytic one). Moreover, one cannot find a single paper in the literature that includes all types of boundary layer problem. In spite of the enormous numerical effort, a truly simple, yet numerically accurate and robust algorithm is still missing. From the review of the schemes proposed in [4-71], two general limitations may be observed:

1. The proposed approximate-analytic methods cannot yield accurate solutions when a rather small number of solution terms are used;
2. Many calculations should be done to construct the resulting semi-analytic solutions, which increase the CPU time considerably, especially when a large number of solution terms are to be used.

The above-mentioned limitations can be eliminated using higher-order methods, such as the Differential Quadrature Method (DQM). The DQM, which was first introduced by Bellman and his associates [72] in the early 1970s, is an alternative efficient discretization technique for solving directly the governing differential equations in engineering and mathematics. Its central idea is to approximate the derivative of a function, with respect to a space/time variable at a given discrete point, by a weighed linear summation of the function values at all of the discrete points in the domain of that variable. Compared to the low-order methods, such as the finite element and finite difference methods, the DQM can generate numerical results with a higher-order of accuracy by using a considerably smaller number of discrete points and, therefore, requiring relatively little computational effort. Another particular advantage of the DQM is its ease of use and implementation. Since its introduction, the DQM has been successfully applied to many areas in engineering and mathematics [73]. Details of this method and references of application of the DQM to various problems may be found, for example, in the review paper by Bert and Malik [74]. More recently, the DQM has been successfully applied to initial-value problems in structural dynamics [75-80]. It has been found that the DQ time integration scheme is reliable, computationally efficient and also suitable for time integrations over a long time duration. Most recently, the DQM has been successfully combined with other approximate methods, such as the Ritz method [81-83] and finite element method [84], and applied to free and forced vibration, and buckling problems of rectangular plates.

The DQM has also been successfully applied to simple boundary layer problems such as the Blasius and Sakiadis equations [85,86]. Liu and Wu [85] proposed the use of Hermite functions as trial functions to determine the weighting coefficients in the DQM and called their method the Generalized Differential Quadrature Method (GDQM). They applied their method to Blasius and Onsager equations and reported accurate solutions. The emphasis on their study was placed on implementing multiple boundary conditions in the solution process. However, as we will show in this paper, the conventional DQM can also produce highly accurate solutions for general boundary layer problems without any difficulty and, thus, there is no need to use any other scheme, such as one proposed by Liu and Wu [85], to implement boundary conditions in the DQ solution of boundary layer equations. On the other hand, Girgin [86] proposed an iterative DQM for solving Blasius and Sakiadis boundary layer problems and called their method the Generalized Iterative Differential Quadrature Method (GIDQM). However, as we know, the proposed method (GIDQM) is, in fact, a direct application of the DQM to boundary layer problems. Moreover, the accuracy and capability of the GIDQM has not been challenged through the solution of general boundary layer problems.

It can be seen that a general formulation based on the DQM for solving general boundary layer problems is still missing. Therefore, the present investigation is devoted to presenting an iterative DQM for the solution of general boundary layer equations. At first, we present a general formulation for solving Blasius, Sakiadis, Falkner-Skan, MHD Falkner-Skan and Jeffery-Hamel boundary layer problems. An iterative DQM will then be presented for solving unsteady two-dimensional and three-dimensional boundary layer problems. Finally, a simple scheme is proposed for solving Blasius boundary layer equation. In this technique, the Blasius boundary value problem is first converted to a pair of initial-value problems [87] and then solved by a step-by-step DQM. A comparison is also made with the conventional fourth-order Runge-Kutta method (RK4).

2. Differential quadrature method

Let $f(\eta,\xi)$ be a solution of a partial differential equation, $\eta_1,\eta_2,\cdots,\eta_n$ be a set of sampling points in the η-direction and $\xi_1,\xi_2,\cdots,\xi_m$ be that in the ξ-direction. According to the DQM, the first-order derivatives, $f_{,\eta}$ and $f_{,\xi}$, at a sample point (η_i,ξ_j) can be expressed by the quadrature rules as [72-74]:

$$f_{,\eta}(\eta_i,\xi_j)=\sum_{k=1}^{n}A_{ik}^{(1)}f_{kj},$$
$$i=1,2,...,n, \tag{14}$$

$$f_{,\xi}(\eta_i,\xi_j)=\sum_{l=1}^{m}B_{jl}^{(1)}f_{il},$$
$$j=1,2,...,m, \tag{15}$$

where $f_{ij}=f(\eta_i,\xi_j)$, $A_{ik}^{(1)}$ are the first-order η-derivative weighting coefficients associated with the $\eta=\eta_i$ point, and, similarly, $B_{jl}^{(1)}$ are the first-order ξ-derivative weighting coefficients associated with the $\xi=\xi_j$ point. $A_{ik}^{(1)}$ and $B_{jl}^{(1)}$ are given by [73]:

$$A_{ik}^{(1)}=\begin{cases}\frac{M^{(1)}(\eta_i)}{(\eta_i-\eta_k)M^{(1)}(\eta_k)} & i\neq k,\\ & i,k=1,2,\cdots,n\\ -\sum_{j=1,j\neq i}^{n}A_{ij}^{(1)} & i=k,\\ & i=1,2,\cdots,n\end{cases} \tag{16}$$

$$B_{jl}^{(1)}=\begin{cases}\frac{M^{(1)}(\xi_j)}{(\xi_j-\xi_l)M^{(1)}(\xi_l)} & j\neq l,\\ & j,l=1,2,\cdots,m\\ -\sum_{i=1,i\neq j}^{m}B_{ji}^{(1)} & j=l,\\ & j=1,2,\cdots,m\end{cases} \tag{17}$$

where $M^{(1)}(\eta)$ and $M^{(1)}(\xi)$ are defined as:

$$M^{(1)}(\eta_i)=\prod_{j=1,j\neq i}^{n}(\eta_i-\eta_j),$$
$$M^{(1)}(\xi_i)=\prod_{j=1,j\neq i}^{m}(\xi_i-\xi_j). \tag{18}$$

The weighting coefficients of the rth-order derivative ($r\geq 2$) may be obtained through the following relationships:

$$A_{ik}^{(r)}=\begin{cases}r\left[A_{ii}^{(r-1)}A_{ik}^{(1)}-\frac{A_{ik}^{(r-1)}}{(\eta_i-\eta_k)}\right] & i\neq k,\\ & i,k=1,2,\cdots,n\\ -\sum_{j=1,j\neq i}^{n}A_{ij}^{(r)} & i=k,\\ & i=1,2,\cdots,n\end{cases} \tag{19}$$

$$B_{jl}^{(r)}=\begin{cases}r\left[B_{jj}^{(r-1)}B_{jl}^{(1)}-\frac{B_{jl}^{(r-1)}}{(\xi_j-\xi_l)}\right] & j\neq l,\\ & j,l=1,2,\cdots,m\\ -\sum_{i=1,i\neq j}^{m}B_{ji}^{(r)} & j=l,\\ & j=1,2,\cdots,m\end{cases} \tag{20}$$

In this study, the sampling points are taken nonuniformly spaced, and are given by the following equations:

$$\eta_i=\frac{\eta^*}{2}\left[1-\cos\left(\frac{(i-1)\pi}{n-1}\right)\right],\qquad i=1,2,\cdots,n, \tag{21}$$

$$\xi_i=\frac{\xi^*}{2}\left[1-\cos\left(\frac{(i-1)\pi}{m-1}\right)\right],\qquad i=1,2,\cdots,m, \tag{22}$$

where η^* and ξ^* are problem boundaries in η- and ξ-directions, respectively.

3. General formulation for steady two-dimensional boundary layer problems

The Blasius, Sakiadis, Falkner-Skan, (MHD) Falkner-Skan and Jeffery-Hamel boundary layer problems all can be described by the following general nonlinear third-order boundary value problem:

$$f'''(\eta)+a_1f(\eta)f''(\eta)+a_2f(\eta)f'(\eta)+a_3f'(\eta)^2+a_4f'(\eta)+a_5=0,\qquad 0\leq\eta\leq\eta^*, \tag{23}$$

subject to the boundary conditions:

$$f(0)=b_1,\qquad f'(0)=b_2,\qquad f(\eta^*)=b_3,\qquad \eta^*=1, \tag{24}$$

for the Jeffery-Hamel boundary layer problem, and:

$$f(0)=b_1,\qquad f'(0)=b_2,\qquad f'(\eta^*)=b_3,$$
$$\eta^*=\infty, \tag{25}$$

for other boundary layer problems. where a_i, b_j ($i=1,\cdots,5$; $j=1,2,3$) are constants.

For the DQ solution of the system equations, Eqs. (23) though (25), first, the requisite quadrature

rules for the first, second and third-order derivatives are written from Eq. (14), as:

$$f'_i = \sum_{j=1}^{n} A^{(1)}_{ij} f_j, \qquad f''_i = \sum_{j=1}^{n} A^{(2)}_{ij} f_j,$$

$$f'''_i = \sum_{j=1}^{n} A^{(3)}_{ij} f_j, \tag{26}$$

wherein:

$$f'_i = f'(\eta_i), \qquad f''_i = f''(\eta_i), \qquad f'''_i = f'''(\eta_i),$$

$$f_j = f(\eta_j), \tag{27}$$

where n is the number of sampling points in the domain $0 \le \eta \le \eta^*$.

Satisfying Eq. (23) at any sample point $\eta = \eta_i$, one has:

$$f'''(\eta_i) + a_1 f(\eta_i) f''(\eta_i) + a_2 f(\eta_i) f'(\eta_i) + a_3 f'(\eta_i)^2 + a_4 f'(\eta_i) + a_5 = 0, \quad i = 1, 2, \cdots, n. \tag{28}$$

Or:

$$f'''_i + a_1 f_i f''_i + a_2 f_i f'_i + a_3 \left(f'_i\right)^2 + a_4 f'_i + a_5 = 0, \quad i = 1, 2, \cdots, n. \tag{29}$$

Now, substituting the quadrature rules given in Eq. (26) into Eq. (29), the quadrature analog of the governing differential equation is obtained as:

$$\sum_{j=1}^{n} A^{(3)}_{ij} f_j + a_1 f_i \sum_{j=1}^{n} A^{(2)}_{ij} f_j + a_2 f_i \sum_{j=1}^{n} A^{(1)}_{ij} f_j + a_3 \left(\sum_{j=1}^{n} A^{(1)}_{ij} f_j \right)^2 + a_4 \sum_{j=1}^{n} A^{(1)}_{ij} f_j + a_5 = 0, \qquad i = 1, 2, \cdots, n. \tag{30}$$

Eq. (30) can be written in matrix notation as:

$$[A]^{(3)}\{f\} + a_1 \{f\} \otimes \left([A]^{(2)}\{f\}\right) + a_2 \{f\} \otimes \left([A]^{(1)}\{f\}\right) + a_3 \left([A]^{(1)}\{f\}\right) \otimes \left([A]^{(1)}\{f\}\right) + a_4 [A]^{(1)}\{f\} + a_5 \{r\} = \{0\}, \tag{31}$$

where:

$$\{f\} = \begin{bmatrix} f_1 & f_2 & \cdots & f_n \end{bmatrix}^T,$$

$$\{r\} = \begin{bmatrix} 1 & 1 & \cdots & 1 \end{bmatrix}^T. \tag{32}$$

Using the quadrature rules, the quadrature analogs of boundary conditions for the Jeffery-Hamel boundary layer equation are obtained as:

$$f_1 = f(\eta_1) = b_1,$$

$$f'_1 = f'(\eta_1) = \sum_{j=1}^{n} A^{(1)}_{1j} f_j = b_2,$$

$$f_n = f(\eta_n) = b_3. \tag{33}$$

Similarly, for other boundary layer equations, they are obtained as:

$$f_1 = f(\eta_1) = b_1,$$

$$f'_1 = f'(\eta_1) = \sum_{j=1}^{n} A^{(1)}_{1j} f_j = b_2,$$

$$f'_n = f'(\eta_n) = \sum_{j=1}^{n} A^{(1)}_{nj} f_j = b_3. \tag{34}$$

After applying the boundary conditions, one can solve the resulting nonlinear system of algebraic equations using various iterative methods for unknowns (function values at the sampling points). In this work, we use the Newton-Raphson method to solve the system (30). Our numerical experiments showed that only 3-5 iterations are sufficient to achieve accurate solutions using the Newton-Raphson method.

Since the Jeffery-Hamel boundary layer problem is defined on a bounded domain ($0 \le \eta \le 1$), the solution to this equation can be easily obtained by solving Eq. (30). However, the solutions to other boundary layer problems (Blasius, Sakiadis, Falkner-Skan and (MHD) Falkner-Skan) cannot be easily obtained, since these problems are defined on an unbounded domain ($0 \le \eta \le 8$) and the position of the far boundary ($\eta = \eta_\infty$) is not known a priori. Thus, the location of the far boundary must also be determined as part of the solutions. The addition of the new unknown, η_∞, to the above-mentioned problems warrants the introduction of the asymptotic condition [3]:

$$f''(\eta) = 0, \qquad \text{at}, \qquad \eta = \eta_\infty. \tag{35}$$

To obtain this unknown (η_∞), one should apply an iterative DQM on the problem domain ($0 \le \eta \le \infty$). The procedure starts with an initial guess, $\eta^* = \eta^*_1$, where η^* is the location of the truncated boundary, and iterates until a desired level of convergence and accuracy is achieved. At the first step, the problem is

solved in the domain $[0, \eta_1^*]$ and, generally, at the pth step in the interval $[0, \eta_p^*]$, where $\eta_p^* = \eta_1^* + (p-1)\Delta\eta^*$ and $\Delta\eta^* = \eta_{p+1}^* - \eta_p^*$. The convergence measure (or convergence criteria) is:

$$\left|f''(\eta_p^*)\right| < \varepsilon, \qquad \text{or,} \qquad \left|f''(\eta_n)\right|_p < \varepsilon, \tag{36}$$

where n is the number of sampling points in the η-direction; p being the iteration number and ε being a small preassigned tolerance value. It should be noted that the above procedure always converges to results larger than true ones (i.e., converges from above). Besides, when $\eta_1^* > \eta_\infty$, the convergence measure may be satisfied at the first step. In this case, one should try to obtain minimum values for η_p^* that satisfy Eq. (36).

The use of the above procedure (with a fixed $\Delta\eta^*$) to determine η_∞ requires a large amount of computational time and, unfortunately, is cumbersome. To overcome this difficulty, one should employ a multi-stage iterative DQM with variable $\Delta\eta^*$ at each stage. In this technique, the search domain in which the iterative scheme is applied becomes narrower and narrower until the desired accuracy is attained. In this technique, at the first stage, the iterative DQM is applied on $[0, \infty]$, with $\Delta\eta^* = 1$, and η_∞^1 is computed (where η_∞^1 is the magnitude of η_∞ obtained at the first stage). At the second stage, iterative DQM is applied on $[\eta_\infty^1 - 0.9, \eta_\infty^1]$, with $\Delta\eta^* = 0.1$, and η_∞^2 is calculated. In general, at the Sth stage, the iterative DQM will be applied on $[\eta_\infty^{S-1} - 9\times 10^{1-S}, \eta_\infty^{S-1}]$, with $\Delta\eta^* = 10^{1-S}$, and η_∞^S will be obtained. Clearly, the number of iterations depends on the required level of accuracy for η_∞. Our numerical experiments showed that the above procedure with 20-50 iterations can predict the location of the truncated boundary accurately. In all computations presented in this paper, the starting value for the η^* is assumed to be $\eta_1^* = 1$.

3.1. Numerical results for Blasius boundary layer problem

Tables 1 and 2 show the convergence behavior of solutions with respect to the number of sampling points (n) for different values of ε. Shown in Tables 1 and 2 are the shear wall stress ($f''0 = \alpha$) and the truncated boundary (η_∞), respectively. It can be seen that the number of sampling points required to achieve accurate solutions depends on the value of ε. For large values of ε, a small number of sampling points can be used to obtain accurate converged solutions. For example, when $\varepsilon \geq 10^{-3}$, the DQM can produce accurate solutions using only 15 sampling points. But, for small values of ε, a large number of sampling points should be used to ensure the accuracy and convergence of solutions. For instance, when $\varepsilon \leq 10^{-5}$, accurate results can be achieved by the proposed method, when $n \geq 25$.

Table 3 shows the computed wall shear stress and truncated boundary obtained by the proposed method and those reported in [32,88]. The number of sampling points (n) and the number of iterations (N) are also shown in this table. It is noted that 'N' is the number of iterations in the multi-stage DQM for calculation of the truncated boundary (say the number of outer iterations). As pointed out earlier, each *outer* iteration involves the solution of a system of nonlinear algebraic equations. Therefore, each outer iteration involves a number of *inner* iterations. Hence, the total number of iterations may become: number of outer iterations × number of inner iterations. However,

Table 1. Convergence of solutions for the wall shear stress $f''(0) = \alpha$ for the Blasius equation.

ε	$n = 15$	$n = 20$	$n = 25$	$n = 30$	$n = 35$	$n = 40$
10^{-2}	0.334	0.334	0.334	0.334	0.334	0.334
10^{-3}	0.3320	0.3322	0.3322	0.3322	0.3322	0.3322
10^{-4}	0.33261	0.33207	0.33207	0.33207	0.33207	0.33207
10^{-5}	0.334536	0.332091	0.332058	0.332059	0.332059	0.332059
10^{-6}	—	0.3321936	0.3320596	0.3320575	0.3320575	0.3320575

Table 2. Convergence of solutions for the truncated boundary η_∞ for the Blasius equation.

ε	$n = 15$	$n = 20$	$n = 25$	$n = 30$	$n = 35$	$n = 40$
10^{-2}	5.26272	5.26271	5.26271	5.26271	5.26271	5.26271
10^{-3}	6.39029	6.39061	6.39061	6.39061	6.39061	6.39061
10^{-4}	7.27654	7.29095	7.29087	7.29087	7.29087	7.29087
10^{-5}	7.98497	8.06655	8.06405	8.06407	8.06407	8.06407
10^{-6}	—	8.75343	8.75238	8.75270	8.75269	8.75269

Table 3. Computed results for the truncated boundary η_∞ and the wall shear stress $f''(0) = \alpha$ for the Blasius equation.

ε	Present				Ref. [32]		Ref. [88]	
	n[a]	N[b]	α	η_∞	α	η_∞	α	η_∞
10^{-2}	15	29	0.334	5.2627	0.335	5.2627	—	—
10^{-3}	18	32	0.332	6.3906	0.332	6.4020	0.332	6.6798
10^{-4}	21	40	0.33207	7.2909	0.33207	7.2909	—	—
10^{-5}	25	28	0.33206	8.0640	0.33206	8.0648	0.33205	8.1847
10^{-6}	29	43	0.3320575	8.7527	0.3320575	8.7527	—	—
10^{-7}	33	44	0.3320573	9.3796	0.3320573	9.3786	0.3320573	9.3867
10^{-8}	37	38	0.332057337	9.9590	0.332057337	9.9589	—	—
10^{-9}	40	40	0.332057336	10.5001	0.332057336	10.5001	0.332057336	10.5764

[a]: Number of DQM sampling points;

[b]: Number of iterations.

Table 4. Convergence of solutions for the wall shear stress $f''(0) = \alpha$ for the Sakiadis equation.

ε	$n = 20$	$n = 25$	$n = 30$	$n = 35$	$n = 40$	$n = 45$
10^{-2}	-0.447	-0.447	-0.447	-0.447	-0.447	-0.447
10^{-3}	-0.444	-0.444	-0.444	-0.444	-0.444	-0.444
10^{-4}	-0.4438	-0.4438	-0.4438	-0.4438	-0.4438	-0.4438
10^{-5}	-0.44427	-0.44373	-0.44375	-0.44375	-0.44375	-0.44375
10^{-6}	-0.444734	-0.443727	-0.443748	-0.443749	-0.443749	-0.443749
10^{-7}	—	-0.4438346	-0.4437360	-0.4437490	-0.4437483	-0.4437483
10^{-8}	—	-0.44393127	-0.44371205	-0.44374908	-0.44374838	-0.44374831

Table 5. Convergence of solutions for the truncated boundary η_∞ for the Sakiadis equation.

ε	$n = 20$	$n = 25$	$n = 30$	$n = 35$	$n = 40$	$n = 45$
10^{-2}	6.17361	6.17361	6.17361	6.17361	6.17361	6.17361
10^{-3}	8.97449	8.97449	8.97449	8.97449	8.97449	8.97449
10^{-4}	11.81115	11.81045	11.81043	11.81043	11.81043	11.81043
10^{-5}	14.66658	14.65723	14.65716	14.65716	14.65716	14.65716
10^{-6}	17.23117	17.48872	17.50560	17.50618	17.50619	17.50619
10^{-7}	—	19.92242	20.34169	20.35558	20.35564	20.35562
10^{-8}	—	20.93044	23.36400	23.22752	23.20622	23.20512

the number of inner iterations in an outer iteration are not equal. Our numerical experiments show that at the first outer iteration, 3-5 inner iterations are required to achieve converged solutions. But, for higher outer iterations, only 2-3 inner iterations are required to obtain converged solutions. Therefore, the total number of iterations in the present method may be estimated as $2N < N_{\text{tot}} < 3N$.

From Table 3, one sees that the present results agree well with those of [32,88]. The present results are found to have closer agreement with the results of [32] than those of [88].

3.2. Numerical results for Sakiadis boundary layer problem

The convergence of solutions for the Sakiadis boundary layer problem is studied in Tables 4 and 5. It can be seen that when a small number of sampling points are used, the convergence and accuracy of the solutions are not very satisfactory for small values of ε. For instance, when $n = 20$, accurate converged solutions can be achieved only for $\varepsilon \geq 10^{-4}$. Note that the solutions with $n = 20$ are not acceptable in accuracy when $\varepsilon \leq 10^{-6}$. The convergence and accuracy of solutions will be improved considerably by increasing

the number of sampling points. In Table 6, the results are compared with the shooting results of Ref. [45]. A good agreement can be seen.

3.3. Numerical results for Falkner-Skan boundary layer problem

In Table 7, the results for wall shear stress and a truncated boundary are compared with those of [32,89]. The present results have closer agreement with the results of [32] than those of [89]. The results for different values of β are given in Table 8. The results of [3,32,88] are also shown for comparison. An excellent agreement can be observed.

3.4. Numerical results for MHD Falkner-Skan boundary layer problem

The numerical results for different types of MHD Falkner-Skan boundary layer are tabulated in Tables 9-11. These results are calculated using $n = 50$ to insure the stability, convergence and accuracy of the solutions.

In Table 9, the present results are compared with the exact, shooting and AMD solution results of [28]. Comparing the results with those of analytical solutions, it is found that the present results are more accurate than the shooting and AMD solutions. It is interesting to note that the present results can match exact data up to 13 decimal digits. These results confirm the high accuracy and efficiency of the proposed procedure for solving boundary layer problems defined on an infinite domain. In Table 10, the present results are compared with those of [35]. It can be seen that the present results have closer agreement with the HAM solution results of [35] than those of other methods. In Table 11, some further comparisons are made with HPM solutions of [55]. A good agreement can be observed.

Table 6. Computed results for the Sakiadis equation ($n = 45$).

η	Present			Shooting [45]		
	$f(\eta)$	$f'(\eta)$	$-f''(\eta)$	$f(\eta)$	$f'(\eta)$	$-f''(\eta)$
0.0	0.00000000	1.00000000	0.44374831	0.00000000	1.0000000	0.44374733
0.5	0.44507728	0.78241753	0.41878277	0.44507720	0.7824172	0.41878160
1.0	0.78620198	0.58715319	0.35831281	0.78620150	0.5871525	0.35831140
5.0	1.57884695	0.02994984	0.02392277	1.57884400	0.0299497	0.02392260
6.17361	1.60163334	0.01168424	0.00939931	—	—	—
8.97449	1.61461504	0.00122014	0.00098550	—	—	—
10	1.61546582	0.00053288	0.00043052	1.61546300	0.0005329	0.00043052
11.81043	1.61597260	0.00012340	0.00009972	—	—	—
14.65716	1.61610999	0.00001236	0.00000999	—	—	—
15	1.61611369	0.00000936	0.00000758	1.61611200	0.0000094	0.00000758
17.50619	1.61612373	0.00000123	0.00000100	—	—	—
20	1.61612503	0.00000015	0.00000013	1.61611200	0.0000001	0.00000013
20.35562	1.61612508	0.00000011	0.00000010	—	—	—
23.20512	1.61612518	0.00000000	0.00000001	—	—	—

Table 7. Computed results for the truncated boundary η_∞ and the wall shear stress $f''(0) = \alpha$ for the Falkner-Skan equation ($\beta_0 = 1$, $\beta = 1/2$).

ε	Present				Ref. [32]		Ref. [89]	
	n[a]	N[b]	α	η_∞	α	η_∞	α	η_∞
10^{-1}	14	32	0.943096	2.216339	0.943096	2.216339	0.943081	2.216707
10^{-2}	17	44	0.928477	3.183995	0.928477	3.183995	0.928476	3.184503
10^{-3}	20	37	0.927733	3.924832	0.927733	3.924832	0.927733	3.925363
10^{-4}	22	37	0.927684	4.543636	0.927684	4.543635	0.927684	4.550585
10^{-5}	25	38	0.927680	5.084267	0.927680	5.084266	0.927680	5.085175
10^{-6}	27	44	0.927680	5.569661	0.927680	5.569661	0.927680	5.571160

[a]: Number of DQM sampling points;

[b]: Number of iterations.

Table 8. Computed results for the truncated boundary η_∞ and the wall shear stress $f''(0) = \alpha$ for the Falkner-Skan equation ($\beta_0 = 1$, $\varepsilon = 10^{-6}$).

β	Present				Ref. [32]		Ref. [88]		Ref. [3]
	n[a]	N[b]	α	η_∞	α	η_∞	α	η_∞	α
40	33	27	7.314785	1.8019	7.314785	1.80	7.314785	1.37	7.314785
30	32	24	6.338209	2.0339	6.338209	2.03	6.338208	1.54	6.338209
20	31	38	5.180718	2.3956	5.180718	2.40	5.180718	1.83	5.180718
15	31	42	4.491487	2.6740	4.491487	2.67	4.491487	2.50	4.491487
10	30	39	3.675234	3.0888	3.675234	3.09	3.675234	2.39	3.675234
2.0	23	43	1.687218	4.6777	1.687218	4.68	1.687218	3.67	1.687218
1.0	23	37	1.232588	5.1876	1.232588	5.19	1.232588	4.30	1.232589
0.5	24	44	0.927680	5.5697	0.927680	5.57	0.927680	4.55	0.927680
0.0	27	38	0.469600	6.2583	0.469600	6.26	0.469600	5.29	0.469600
-0.1	30	34	0.319270	6.5494	0.319270	6.55	0.319270	5.56	0.319270
-0.15	32	38	0.216362	6.7883	0.216362	6.79	0.216362	5.79	0.216361
-0.18	32	28	0.128637	7.0347	0.128637	7.03	0.128637	6.03	0.128637
-0.1988	36	28	0.005229	7.5104	0.005229	7.51	0.005226	6.68	0.005225

[a]: Number of DQM sampling points; [b]: Number of iterations.

Table 9. Computed results for the truncated boundary η_∞ and $f'(1)$ for the MHD Falkner-Skan equation[a] ($n = 50$, $\varepsilon = 10^{-12}$).

f_w	M	k_p	Present			Exact [28]	Shooting [28]	AMD [28]
			N[b]	$f'(1)$	η_∞	$f'(1)$	$f'(1)$	$f'(1)$
0.1	0.5	5	35	0.2579991896208	20.601002	0.2579991896208	0.2580018814864	0.2579991264067
0.4	0.5	5	35	0.2189108749214	18.500132	0.2189108749214	0.2189120624529	0.2189108467711
0.7	0.5	5	49	0.1826835240527	16.036028	0.1826835240527	0.1826846008492	0.1826835145613
0.1	1.0	5	31	0.2156535254584	18.500101	0.2156535254584	0.2156547493061	0.2156535231532
0.1	1.5	5	59	0.1837961120799	16.410206	0.1837961120799	0.1837972387054	0.1837961119397
0.1	0.5	1	59	0.1955519507823	17.064271	0.1955519507823	0.1955532080746	0.1955519503997
0.1	0.5	1.5	28	0.2180983639145	19.011001	0.2180983639145	0.2180996387404	0.2180983610746
0.1	0.5	2	33	0.2310555387640	19.300032	0.2310555387640	0.2310569393893	0.2310555305671

[a]: $f'''(\eta) + f(\eta)f''(\eta) - f'(\eta)^2 - (M + 1/k_p)f'(\eta) = 0$, $f(0) = f_w$, $f'(0) = 1$, $f'(\infty) = 1$; [b]: Number of iterations.

Table 10. Computed results for the truncated boundary η_∞ and the wall shear stress $f''(0) = \alpha$ for the MHD Falkner-Skan equation[a] ($n = 50$, $\varepsilon = 10^{-8}$).

β	M	Present			HAM [35]	Crocco [35]	Shooting [35]
		N[b]	α	η_∞	α	α	α
4/3	1	37	1.71946568	5.590004	1.71947219	1.71076376	1.71946540
	2	23	2.43949896	5.027111	2.43949870	2.43348047	2.43949833
	5	30	5.19095980	3.391341	5.19095980	5.18824018	5.19095945
	10	18	10.09677575	2.017002	10.09677575	10.09539387	10.09677545
	50	25	50.01944084	0.458002	50.01944084	50.01916312	50.01944071
	100	24	100.00972177	0.236502	100.00972177	100.00958289	100.00972170
-3	3	21	2.27338480	5.630001	2.27338419	2.26555724	2.27338836
	4	24	3.48814584	4.561011	3.48814572	3.48374014	3.48814857
	5	31	4.60075228	3.826141	4.60075228	4.59755490	4.60075494
	10	22	9.80646300	2.094001	9.80646300	9.80502889	9.80646420
	15	27	14.87167401	1.439103	14.87167401	14.87073502	14.87167484
	20	10	19.90393626	1.100002	19.90393626	19.90323635	19.90393701
	50	28	49.96165198	0.459013	49.96165198	49.96137386	49.96165233

[a]: See Eq. (4); [b]: Number of iterations.

Table 11. Computed results for the truncated boundary η_∞ and the wall shear stress $f''(0) = \alpha$ for the MHD Falkner-Skan equation[a] ($n = 50$, $\varepsilon = 10^{-8}$).

β	M	Present			HPM [55]	M-HPM [55]	Exact [55]
		N[b]	$-\alpha$	η_∞	$-\alpha$	$-\alpha$	$-\alpha$
1	0	45	1.00000000	18.420654	1.00000	1.00000	1.00000
	1	39	1.41421356	13.557201	1.41421	1.41421	1.41421
	5	35	2.44948974	8.133321	2.44948	2.44948	2.44948
	10	21	3.31662479	6.110511	3.31662	3.31662	3.31662
	50	37	7.14142843	2.950339	7.14142	7.14142	7.14142
	100	16	10.04987562	2.131021	10.0499	10.0499	10.04987
	500	38	22.38302929	0.992741	22.383	22.383	22.38302
	1000	29	31.63858404	0.713291	31.6386	31.6386	31.63858

[a]: $f'''(\eta) + f(\eta)f''(\eta) - \beta f'(\eta)^2 - Mf'(\eta) = 0$, $f(0) = 0$, $f'(0) = 1$, $f'(\infty) = 0$;

[b]: Number of iterations.

Table 12. Computed results for the function $f(\eta)$ for the Jeffery-Hamel equation[a] (Ha = 0, Re = 110, $\alpha = 3^\circ$).

η	Present			HAM [71]	Runge-Kutta [71]
	$n = 20$	$n = 25$	$n = 30$		
0.0	1.000000000000	1.000000000000	1.000000000000	1.0000000000	1.0000000000
0.1	0.979235706518	0.979235706523	0.979235706523	0.9792357062	0.9792357085
0.2	0.919265885575	0.919265885585	0.919265885585	0.9192658842	0.9192658898
0.3	0.826533612270	0.826533612283	0.826533612283	0.8265336102	0.8265336182
0.4	0.710221183224	0.710221183238	0.710221183238	0.7102211838	0.7102211890
0.5	0.580499458790	0.580499458804	0.580499458804	0.5804994700	0.5804994634
0.6	0.446935067029	0.446935067042	0.446935067042	0.4469350941	0.4469350697
0.7	0.317408427566	0.317408427577	0.317408427577	0.3174084545	0.3174084270
0.8	0.197641094520	0.197641094528	0.197641094528	0.1976410661	0.1976410889
0.9	0.091230421094	0.091230421098	0.091230421098	0.09123022879	0.0912304211
1.0	0.000000000000	0.000000000000	0.000000000000	-0.00000047	0.0000000000

[a]: See Eq. (12)

3.5. Numerical results for Jeffery-Hamel boundary layer problem

The numerical results for the Jeffery-Hamel boundary layer problem with different values of α, Re and Ha (defined in Eq. (12)) are shown in Tables 12-14. Tables 12 and 13 show the converging trend of the solutions, with respect to the number of sampling points. It is interesting to note that the present results may converge to 13 significant figures for a small grid size of $n = 25$. From Tables 12 and 13, one also sees that the present results have closer agreement with Runge-Kutta solutions than the HAM solutions. In Table 14, the results are compared with VIM and Runge-Kutta solutions of [67]. It can be seen that the present results are in closer agreement with Runge-Kutta solutions than VIM solutions.

4. Formulation for unsteady two-dimensional boundary layer problems

Consider the unsteady two-dimensional boundary layer flow on a fixed or moving flat surface. The governing non-dimensional equation for boundary layer flow is given in Eq. (6). The boundary conditions are:

$$f(0,\xi) = c_1,$$

$$f_{,\eta}(0,\xi) = c_2,$$

$$f_{,\eta}(\eta^*,\xi) = c_3, \tag{37}$$

where $c_i (i = 1, 2, 3)$ are constants. For the differential quadrature solution of Eq. (6), consider a grid of $n \times m$ sampling points obtained by taking n and m points in

Table 13. Computed results for the function $f(\eta)$ for the Jeffery-Hamel equation[a] (Ha = 1000, Re = 50, $\alpha = -5°$).

η	Present			HAM [69]	Runge-Kutta [69]
	$n = 20$	$n = 25$	$n = 30$		
0.0	1.000000000000	1.000000000000	1.000000000000	1.0000000000	1.0000000000
0.1	0.996756698152	0.996756698170	0.996756698170	0.9967570409	0.9967567004
0.2	0.986491485791	0.986491485822	0.986491485822	0.9864928100	0.9864914948
0.3	0.967516559607	0.967516559647	0.967516559647	0.9675193145	0.9675165808
0.4	0.936737943318	0.936737943362	0.936737943362	0.9367421766	0.9367379265
0.5	0.889208363043	0.889208363089	0.889208363089	0.8892135408	0.8892083429
0.6	0.817461287392	0.817461287437	0.817461287437	0.8174664644	0.8174612678
0.7	0.710623416794	0.710623416836	0.710623416836	0.7106275597	0.7106233991
0.8	0.553387469139	0.553387469173	0.553387469173	0.5533900638	0.5533874550
0.9	0.325141357717	0.325141357738	0.325141357738	0.3251423732	0.3251413493
1.0	0.000000000000	0.000000000000	0.000000000000	0.0000000000	0.0000000000

[a]: See Eq. (12).

Table 14. Computed results for the Jeffery-Hamel equation[a] (Ha = 0, Re = 50, $\alpha = 5°$, $n = 25$).

n	Present		VIM [67]		Runge-Kutta [67]	
	$f(\eta)$	$f''(\eta)$	$f(\eta)$	$f''(\eta)$	$f(\eta)$	$f''(\eta)$
0.0	1.00000000	-3.53941563	1.000000	-3.539369	1.000000	-3.539416
0.1	0.98243124	-3.38691089	0.982431	-3.386866	0.982431	-3.386911
0.2	0.93122596	-2.95779189	0.931227	-2.957753	0.931226	-2.957792
0.3	0.85061062	-2.32857378	0.850613	-2.328542	0.850611	-2.328574
0.4	0.74679080	-1.60178937	0.746794	-1.601767	0.746791	-1.601789
0.5	0.62694817	-0.87979398	0.626953	-0.879791	0.626948	-0.879794
0.6	0.49823445	-0.24394857	0.498241	-0.243994	0.498234	-0.243949
0.7	0.36696634	0.25560697	0.366974	0.255470	0.366966	0.255607
0.8	0.23812375	0.59970242	0.238131	0.599464	0.238124	0.599702
0.9	0.11515193	0.79300399	0.115157	0.792767	0.115152	0.793004
1.0	0.00000000	0.85436924	0.000000	0.854401	0.000000	0.854369

[a]: See Eq. (12).

$0 \le \xi \le \xi^*$ and $0 \le \eta \le \eta^*$, respectively. Satisfying Eq. (6) at any sample point (η_i, ξ_j), one has:

$$\begin{aligned} & f_{,\eta\eta\eta}(\eta_i,\xi_j) + \frac{1}{2}(1-\xi_j)\eta_i f_{,\eta\eta}(\eta_i,\xi_j) \\ & \quad + \xi_j\left[f(\eta_i,\xi_j)f_{,\eta\eta}(\eta_i,\xi_j) - f^2_{,\eta}(\eta_i,\xi_j)\right] \\ & \quad = \xi_j(1-\xi_j)f_{,\eta\xi}(\eta_i,\xi_j), \end{aligned}$$

$$i = 1, 2, \cdots, n, \qquad j = 1, 2, \cdots, m. \tag{38}$$

Now, using the quadrature rules, the quadrature analog of Eq. (38) is obtained as:

$$\begin{aligned} & \sum_{k=1}^{n} A^{(3)}_{ik} f_{kj} + \frac{1}{2}(1-\xi_j)\eta_i \sum_{k=1}^{n} A^{(2)}_{ik} f_{kj} \\ & \quad + \xi_j\left[f_{ij}\sum_{k=1}^{n} A^{(2)}_{ik} f_{kj} - \left(\sum_{k=1}^{n} A^{(1)}_{ik} f_{kj}\right)^2\right] \\ & \quad = \xi_j(1-\xi_j)\sum_{k=1}^{n}\sum_{l=1}^{m} A^{(1)}_{ik} B^{(1)}_{jl} f_{kl,}, \end{aligned}$$

$$i = 1, 2, \cdots, n, \qquad j = 1, 2, \cdots, m. \tag{39}$$

Similarly, the quadrature analogs of boundary conditions are written as:

$$f_{1j} = f(\eta_1, \xi_j) = c_1, \qquad j = 1, 2, \cdots, m, \tag{40}$$

$$f_{,\eta}(\eta_1, \xi_j) = \sum_{k=1}^{n} A_{1k}^{(1)} f_{kj} = c_2, \qquad j = 1, 2, \cdots, m, \tag{41}$$

$$f_{,\eta}(\eta_n, \xi_j) = \sum_{k=1}^{n} A_{nk}^{(1)} f_{kj} = c_3, \qquad j = 1, 2, \cdots, m. \tag{42}$$

Using Eqs. (40)-(42) in Eq. (39), the boundary conditions can be invoked into the quadrature analog of the differential equation. Then, an iterative scheme similar to that described in Section 3 can be used to obtain the truncated boundary and the solution of the unsteady two-dimensional boundary layer problem. Note that the unsteady two-dimensional boundary layer flow is also subjected to the following asymptotic boundary condition:

$$f_{,\eta\eta}(\eta, \xi) = 0 \qquad \text{at} \qquad (\eta, \xi) = (\eta_\infty, \xi). \tag{43}$$

Therefore, the convergence criteria for this case become:

$$\left|f_{,\eta\eta}(\eta_p^*, \xi)\right| < \varepsilon \qquad \text{or} \qquad \left|f_{,\eta\eta}(\eta_n, \xi)\right|_p < \varepsilon, \tag{44}$$

where p is the iteration number, while n is the total number of sampling points in the η-direction. The above criteria should be satisfied at $\xi_1, \xi_2, \cdots, \xi_m$. Therefore, to check the accuracy and convergence of the solutions, it is sufficient to satisfy the following criteria:

$$\max_{1 \le j \le m} \left|f_{,\eta\eta}(\eta_p^*, \xi_j)\right| < \varepsilon \qquad \text{or}$$

$$\max_{1 \le j \le m} \left|f_{,\eta\eta}(\eta_n, \xi_j)\right|_p < \varepsilon. \tag{45}$$

4.1. Numerical results

To demonstrate the efficiency and accuracy of the proposed algorithm, application is made to a numerical example given by Liao [59]. A convergence study is first made to determine proper values of n (number of sampling points in the η-direction) and m (number of sampling points in the ξ-direction) for discretization of the problem domain and for accurate solution of the boundary layer problem. The results for wall shear stresses ($f_{,\eta\eta}(0,0) = \alpha$), with $\varepsilon = 10^{-3}$, are given in Table 15. It can be seen that accurate converged results are achieved by the present method with $n = 15$ and $m = 2$. Note that $m = 2$ is the smallest number of sampling points that can be used in the proposed method for solving the present problem.

In Table 16, the results for wall shear stress and truncated boundary are given for various values of ε. The analytic solutions of [59] are also shown for comparison purposes. It can be seen that the present results are matching with exact solutions to an excellent extent. These results confirm the high accuracy and efficiency of the proposed procedure for solving unsteady boundary layer problems defined on an infinite domain.

Table 15. Convergence of solutions for the wall shear stress $f_{,\eta\eta}(0,0) = \alpha$ for the unsteady two-diensional boundary layer problem[a] ($\varepsilon = 10^{-3}$).

m[b]	n[c] = 12	$n = 15$	$n = 19$	$n = 24$	$n = 27$	$n = 30$
2	-0.566	-0.564	-0.564	-0.564	-0.564	-0.564
3	-0.566	-0.564	-0.564	-0.564	-0.564	-0.564
4	-0.566	-0.564	-0.564	-0.564	-0.564	-0.564
5	-0.566	-0.564	-0.564	-0.564	-0.564	-0.564
6	-0.566	-0.564	-0.564	-0.564	-0.564	-0.564
7	-0.566	-0.564	-0.564	-0.564	-0.564	-0.564

[a]: See Eq. (6);

[b]: Number of DQM sampling points in ξ-direction;

[c]: Number of DQM sampling points in η-direction.

5. Formulation for unsteady three-dimensional boundary layer problems

Consider the unsteady three-dimensional boundary layer flow on a fixed or moving flat surface. The governing non-dimensional equation for boundary layer flow is given in Eqs. (8)-(10). The boundary conditions are:

$$f(0, \xi) = d_1, \qquad f_{,\eta}(0, \xi) = d_2, \qquad f_{,\eta}(\eta^*, \xi) = d_3, \tag{46}$$

Table 16. Computed results for the truncated boundary η_∞ and the wall shear stress $f_{,\eta\eta}(0,0) = \alpha$ for the unsteady two-diensional boundary layer problem[a] ($m = 4$).

ε	Present				Exact[d] [59]
	n[b]	N[c]	$-\alpha$	η_∞	$-\alpha$
10^{-1}	10	27	0.6	2.676	0.6
10^{-2}	14	27	0.566	4.186	0.564
10^{-3}	15	33	0.564	5.393	0.564
10^{-4}	16	30	0.5642	6.393	0.5642
10^{-5}	19	33	0.56419	7.265	0.56419
10^{-6}	23	30	0.564190	8.048	0.564190
10^{-7}	28	39	0.5641896	8.765	0.5641896
10^{-8}	31	30	0.56418958	9.431	0.56418958
10^{-9}	32	24	0.564189584	10.054	0.564189584
10^{-10}	38	33	0.56418958355	10.631	0.56418958355

[a]: See Eq. (6);

[b]: Number of DQM sampling points in η-direction;

[c]: Number of iterations;

[d]: Exact value from [59] is $-1/\sqrt{\pi}$.

$$s(0,\xi)=d_4,\qquad s_{,\eta}(0,\xi)=d_5,\qquad s_{,\eta}(\eta^*,\xi)=d_6, \tag{47}$$

$$g(0,\xi)=d_7,\qquad g(\eta^*,\xi)=d_8, \tag{48}$$

where $d_i (i=1,\cdots,8)$ are constants. Satisfying Eqs. (8)-(10) at any sample point (η_i,ξ_j), one has $(i=1,2,\cdots,n,\ j=1,2,\cdots,m)$:

$$\begin{aligned} f_{,\eta\eta\eta}(\eta_i,\xi_j)+\frac{1}{2}(1-\xi_j)\eta_i f_{,\eta\eta}(\eta_i,\xi_j)+\xi_j[(f(\eta_i,\xi_j)\\ +s(\eta_i,\xi_j))f_{,\eta\eta}(\eta_i,\xi_j)-f^2_{,\eta}(\eta_i,\xi_j)\\ -Mf_{,\eta}(\eta_i,\xi_j)]=\xi_j(1-\xi_j)f_{,\eta\xi}(\eta_i,\xi_j), \end{aligned} \tag{49}$$

$$\begin{aligned} s_{,\eta\eta\eta}(\eta_i,\xi_j)+\frac{1}{2}(1-\xi_j)\eta_i s_{,\eta\eta}(\eta_i,\xi_j)+\xi_j[(f(\eta_i,\xi_j)\\ +s(\eta_i,\xi_j))s_{,\eta\eta}(\eta_i,\xi_j)-s^2_{,\eta}(\eta_i,\xi_j)\\ -Ms_{,\eta}(\eta_i,\xi_j)]=\xi_j(1-\xi_j)s_{,\eta\xi}(\eta_i,\xi_j), \end{aligned} \tag{50}$$

$$\begin{aligned} g_{,\eta\eta}(\eta_i,\xi_j)+\frac{1}{2}\mathrm{Pr}(1-\xi_j)\eta_i g_{,\eta}(\eta_i,\xi_j)\\ +\mathrm{Pr}\xi_j(f(\eta_i,\xi_j)+s(\eta_i,\xi_j))g_{,\eta}(\eta_i,\xi_j)\\ =\mathrm{Pr}\xi_j(1-\xi_j)g_{,\xi}(\eta_i,\xi_j). \end{aligned} \tag{51}$$

Now, using the quadrature rules, the quadrature analogs of Eqs. (49)-(51) are obtained as $(i=1,2,\cdots,n,\ j=1,2,\cdots,m)$:

$$\begin{aligned} \sum_{k=1}^{n}A^{(3)}_{ik}f_{kj}+\frac{1}{2}(1-\xi_j)\eta_i\sum_{k=1}^{n}A^{(2)}_{ik}f_{kj}\\ +\xi_j\left[(f_{ij}+s_{ij})\sum_{k=1}^{n}A^{(2)}_{ik}f_{kj}\right.\\ \left.-\left(\sum_{k=1}^{n}A^{(1)}_{ik}f_{kj}\right)^2-M\sum_{k=1}^{n}A^{(1)}_{ik}f_{kj}\right]\\ =\xi_j(1-\xi_j)\sum_{k=1}^{n}\sum_{l=1}^{m}A^{(1)}_{ik}B^{(1)}_{jl}f_{kl}, \end{aligned} \tag{52}$$

$$\begin{aligned} \sum_{k=1}^{n}A^{(3)}_{ik}s_{kj}+\frac{1}{2}(1-\xi_j)\eta_i\sum_{k=1}^{n}A^{(2)}_{ik}s_{kj}\\ +\xi_j\left[(f_{ij}+s_{ij})\sum_{k=1}^{n}A^{(2)}_{ik}s_{kj}\right.\\ \left.-\left(\sum_{k=1}^{n}A^{(1)}_{ik}s_{kj}\right)^2-M\sum_{k=1}^{n}A^{(1)}_{ik}s_{kj}\right]\\ =\xi_j(1-\xi_j)\sum_{k=1}^{n}\sum_{l=1}^{m}A^{(1)}_{ik}B^{(1)}_{jl}s_{kl}, \end{aligned} \tag{53}$$

$$\begin{aligned} \sum_{k=1}^{n}A^{(2)}_{ik}g_{kj}+\frac{1}{2}\mathrm{Pr}(1-\xi_j)\eta_i\sum_{k=1}^{n}A^{(1)}_{ik}g_{kj}\\ +\mathrm{Pr}\xi_j(f_{ij}+s_{ij})\sum_{k=1}^{n}A^{(1)}_{ik}g_{kj}\\ =\mathrm{Pr}\xi_j(1-\xi_j)\sum_{l=1}^{m}B^{(1)}_{jl}g_{il}. \end{aligned} \tag{54}$$

Similarly, the quadrature analogs of boundary conditions are written as $(j=1,2,\cdots,m)$.

$$\begin{aligned} f_{1j}&=f(\eta_1,\xi_j)=d_1,\\ s_{1j}&=s(\eta_1,\xi_j)=d_4,\\ g_{1j}&=g(\eta_1,\xi_j)=d_7, \end{aligned} \tag{55}$$

$$\begin{aligned} f_{,\eta}(\eta_1,\xi_j)&=\sum_{k=1}^{n}A^{(1)}_{1k}f_{kj}=d_2,\\ s_{,\eta}(\eta_1,\xi_j)&=\sum_{k=1}^{n}A^{(1)}_{1k}s_{kj}=d_5, \end{aligned} \tag{56}$$

$$\begin{aligned} f_{,\eta}(\eta_n,\xi_j)&=\sum_{k=1}^{n}A^{(1)}_{nk}f_{kj}=d_3,\\ s_{,\eta}(\eta_n,\xi_j)&=\sum_{k=1}^{n}A^{(1)}_{nk}s_{kj}=d_6,\\ g_{,\eta}(\eta_n,\xi_j)&=\sum_{k=1}^{n}A^{(1)}_{nk}g_{kj}=d_8. \end{aligned} \tag{57}$$

Using Eqs. (55)-(57) in Eqs. (52)-(54), the boundary conditions can be invoked into the quadrature analog of the differential equation. Then, a similar iterative scheme to that described in Section 4 can be used to obtain the truncated boundary and the solution of the unsteady three-dimensional boundary layer problem.

5.1. Numerical results

To demonstrate the efficiency of the proposed algorithm, application is made to a numerical example given by Kumari and Nath [61]. Tables 17 and 18 present the convergence of solutions for the truncated boundary (η_∞) and wall shear stress ($f_{,\eta\eta}(0,1)=\alpha$),

Table 17. Convergence of solutions for the truncated boundary η_∞ for the unsteady three-dimensional boundary layer problem[a] ($M = 0$, $\varepsilon = 10^{-5}$).

c	m[b]	n[c] $= 20$	$n = 23$	$n = 25$	$n = 28$	$n = 31$	$n = 35$
0.25	2	10.10968	10.11155	10.11160	10.11163	10.11163	10.11163
	3	10.10968	10.11155	10.11160	10.11163	10.11163	10.11163
	4	10.10968	10.11155	10.11160	10.11163	10.11163	10.11163
	5	10.10968	10.11155	10.11160	10.11163	10.11163	10.11163
0.50	2	9.23031	9.23371	9.23384	9.23391	9.23391	9.23391
	3	9.23031	9.23371	9.23384	9.23391	9.23391	9.23391
	4	9.23031	9.23371	9.23384	9.23391	9.23391	9.23391
	5	9.23031	9.23371	9.23384	9.23391	9.23391	9.23391
0.75	2	8.59079	8.59556	8.59577	8.59587	8.59587	8.59587
	3	8.59079	8.59556	8.59577	8.59587	8.59587	8.59587
	4	8.59079	8.59556	8.59577	8.59587	8.59587	8.59587
	5	8.59079	8.59556	8.59577	8.59587	8.59587	8.59587

[a]: See Eqs. (8-11);

[b]: Number of DQM sampling points in ξ-direction;

[c]: Number of DQM sampling points in η-direction.

Table 18. Convergence and comparison of solutions for the wall shear stress $f_{,\eta\eta}(0,1) = \alpha$ for the unsteady three-dimensional boundary layer problem[a] ($M = 0$, $\varepsilon = 10^{-5}$).

c	m[b]	n[c] $= 20$	$n = 23$	$n = 25$	$n = 28$	$n = 31$	$n = 35$	HAM [61]
0.25	2	-1.04881	-1.04882	-1.04881	-1.04881	-1.04881	-1.04881	-1.04901
	3	-1.04881	-1.04882	-1.04881	-1.04881	-1.04881	-1.04881	
	4	-1.04881	-1.04882	-1.04881	-1.04881	-1.04881	-1.04881	
	5	-1.04881	-1.04882	-1.04881	-1.04881	-1.04881	-1.04881	
0.50	2	-1.09310	-1.09311	-1.09310	-1.09310	-1.09310	-1.09310	-1.09346
	3	-1.09310	-1.09311	-1.09310	-1.09310	-1.09310	-1.09310	
	4	-1.09310	-1.09311	-1.09310	-1.09310	-1.09310	-1.09310	
	5	-1.09310	-1.09311	-1.09310	-1.09310	-1.09310	-1.09310	
0.75	2	-1.13451	-1.13451	-1.13449	-1.13449	-1.13449	-1.13449	-1.13491
	3	-1.13451	-1.13451	-1.13449	-1.13449	-1.13449	-1.13449	
	4	-1.13451	-1.13451	-1.13449	-1.13449	-1.13449	-1.13449	
	5	-1.13451	-1.13451	-1.13449	-1.13449	-1.13449	-1.13449	

[a]: See Eqs. (8-11);

[b]: Number of DQM sampling points in ξ-direction;

[c]: Number of DQM sampling points in η-direction.

with n and m, for three different values of c (see Eq. (11) for details). The HAM solutions of [61] are also included for comparison. It can be seen from Tables 17 and 18 that the present method can produce accurate converged solutions with $n = 28$ and $m = 2$.

In Table 19, the results for the truncated boundary, η_∞, and the wall shear stresses, $f_{,\eta\eta}(0,1) = \alpha$ and $s_{,\eta\eta}(0,1) = \beta$, are compared with those of [61,90]. The agreement between the results of the present method and those of [61,90] is excellent. In Table 20, the convergence and accuracy of solutions for $g_{,\eta}(0,1) = \gamma$ are studied. The results are compared with numerical and HAM solutions of [61]. It can be seen that the results of the proposed formulation converge very quickly and agree well with those of [61]. These results confirm the correctness of the proposed procedure for solving unsteady three-dimensional boundary layer problems.

Table 19. Computed results for the truncated boundary η_∞ and the wall shear stresses $f_{,\eta\eta}(0,1)=\alpha$, $s_{,\eta\eta}(0,1)=\beta$ for the unsteady three-dimensional boundary layer problem[a] ($M=0$, $\varepsilon=10^{-5}$, $n=31$, $m=2$).

	Present				Ref. [90]		Ref. [61]	
c	N[b]	$-\alpha$	$-\beta$	$-\eta_\infty$	$-\alpha$	$-\beta$	$-\alpha$	$-\beta$
0.0	41	1.00000	0.00000	11.51352	1.00000	0.00000	1.00000	0.00000
0.1	52	1.02026	0.06685	10.85150	1.02025	0.06684	1.02026	0.06685
0.2	42	1.03950	0.14874	10.33381	1.03949	0.14873	1.03950	0.14874
0.3	43	1.05796	0.24336	9.90832	1.05795	0.24335	1.05796	0.24336
0.4	48	1.07579	0.34921	9.54726	1.07578	0.34920	1.07580	0.34922
0.5	38	1.09310	0.46521	9.23391	1.09309	0.46520	1.09311	0.46521
0.6	55	1.10995	0.59053	8.95739	1.10994	0.59052	1.10995	0.59053
0.7	31	1.12640	0.72453	8.71021	1.12639	0.72453	1.12640	0.72455
0.8	54	1.14249	0.86669	8.48696	1.14248	0.86668	1.14250	0.86670
0.9	37	1.15826	1.01654	8.28361	1.15825	1.01653	1.15827	1.01655
1.0	46	1.17372	1.17372	8.09709	1.17372	1.17372	1.17374	1.17374

[a]: See Eqs. (8-11);

[b]: Number of iterations.

Table 20. Convergence and comparison of solutions for $g_{,\eta}(0,1)=\gamma$ for the unsteady three-dimensional boundary layer problem[a] ($M=0$, $\Pr=0.7$, $\varepsilon=10^{-5}$, $m=2$).

	Present					Numeric [61]	HAM [61]
c	$m=20$	$m=23$	$m=25$	$m=28$	$m=31$		
0.0	-0.45410	-0.45410	-0.45410	-0.45410	-0.45410	-0.45446	-0.45465
0.25	-0.52104	-0.52104	-0.52104	-0.52104	-0.52104	-0.52111	-0.52136
0.5	-0.57585	-0.57585	-0.57585	-0.57585	-0.57585	-0.57582	-0.57603
0.75	-0.62391	-0.62391	-0.62391	-0.62391	-0.62391	-0.62383	-0.62406
1.0	-0.66744	-0.66743	-0.66743	-0.66743	-0.66743	-0.66734	-0.66757

[a]: See Eqs. (8)-(11).

6. Solution of the Blasius boundary layer equation by reducing Blasius boundary value problem to a pair of initial-value problems

The Blasius boundary value problem can be reduced to a pair of initial value problems by means of a group of transformations [87]. The initial value problems are given by:

$$g'''(\xi)+\frac{1}{2}g(\xi)g''(\xi)=0, \tag{58}$$

with initial conditions:

$$g(0)=g'(0)=0, \qquad g''(0)=1. \tag{59}$$

And:

$$f'''(\xi)+\frac{1}{2}f(\xi)f''(\xi)=0, \tag{60}$$

with initial conditions:

$$f(0)=f'(0)=0, \qquad f''(0)=[g'(\infty)]^{-3/2}. \tag{61}$$

These equations suggest a transformation of the form [87]:

$$g(\xi)=\lambda^{-1/3}f(\eta), \qquad \xi=\lambda^{1/3}\eta,$$

$$\lambda=[g'(\infty)]^{-3/2}. \tag{62}$$

It is noted that $g(\xi)$ is a bounded continuous function and, thus, $g'(\infty)$ does exist. Let:

$$g'(\infty)=\lim_{\xi\to\infty}g'(\xi)=L. \tag{63}$$

It can be seen that if we solve Eq. (58) for $g(\xi)$ and determine the magnitude of L, then we can obtain the solution of the Blasius equation from Eq. (60).

6.1. DQ analogs of resulting initial value problems

The initial value problems given in Eqs. (58) and (60) can both be described by the following general initial

value problem:

$$\dddot{F}(t) + \frac{1}{2}F(t)\ddot{F}(t) = 0, \tag{64}$$

with initial conditions:

$$F(0) = F_0, \qquad \dot{F}(0) = \dot{F}_0, \qquad \ddot{F}(0) = \ddot{F}_0, \tag{65}$$

where F_0, $\dot{F}_0$ and $\ddot{F}_0$ are constants.

The third-order initial-value problem (Eq. (64)) can be converted into a set of first-order initial-value problems as in the following:

$$\begin{cases} \dot{x} = y \\ \dot{y} = z \\ \dot{z} = -\frac{1}{2}xz \end{cases} \tag{66}$$

with initial conditions:

$$x(0) = F_0, \qquad y(0) = \dot{F}_0, \qquad z(0) = \ddot{F}_0. \tag{67}$$

From the quadrature rule, Eq. (14), the first-order derivative of functions x, y, and z can be expressed as:

$$\dot{x}_i = \sum_{j=1}^{m} A_{ij}^{(1)} x_j, \qquad \dot{y}_i = \sum_{j=1}^{m} A_{ij}^{(1)} y_j,$$

$$\dot{z}_i = \sum_{j=1}^{m} A_{ij}^{(1)} z_j, \qquad i = 1, 2, \cdots, m. \tag{68}$$

Satisfying Eq. (66) at any sample time point, $t = t_i$, and substituting the quadrature rules given in Eq. (68) into results, gives:

$$\begin{cases} \sum\limits_{j=1}^{m} A_{ij}^{(1)} x_j = y_i \\ \sum\limits_{j=1}^{m} A_{ij}^{(1)} y_j = z_i \qquad i = 1, 2, \cdots, m \\ \sum\limits_{j=1}^{m} A_{ij}^{(1)} z_j = -\frac{1}{2}x_i z_i \end{cases} \tag{69}$$

Applying the initial conditions (given in Eq. (67)) in Eq. (69) yields:

$$\begin{cases} \sum\limits_{j=2}^{m} A_{ij}^{(1)} x_j + A_{i1}^{(1)} F_0 = y_i \\ \sum\limits_{j=2}^{m} A_{ij}^{(1)} y_j + A_{i1}^{(1)} \dot{F}_0 = z_i \qquad i = 2, 3, \cdots, m \\ \sum\limits_{j=2}^{m} A_{ij}^{(1)} z_j + A_{i1}^{(1)} \ddot{F}_0 = -\frac{1}{2}x_i z_i \end{cases} \tag{70}$$

Clearly, Eq. (70) is a nonlinear system of algebraic equations which can be solved using various iterative methods. In this study, we used the Newton-Raphson method to solve the system (70). Again we observed that only 3-5 iterations are sufficient to achieve accurate solutions using the Newton-Raphson method.

6.2. A step-by-step DQ in time

For initial value problems, if the while time domain of interest is discretized simultaneously, many unknowns have to be solved simultaneously. As a result, it is more convenient to apply the DQM as a step-by-step time integration scheme to advance the solutions progressively over the time domain of interest [75-80]. In this technique, the time domain of interest is first divided into a number of time elements. The DQM is then applied to each time element independently. The results at the end of each time element will then be used as initial conditions for the next time element (for more details, see [75-80]).

6.3. Numerical results and discussion

As mentioned earlier, we should first determine the magnitude of L (defined in Eq. (63)). This parameter can be obtained using the solution of Eq. (58). To solve Eq. (58) using the scheme described in Section 6.2, we divide the time domain into n_T equal length DQM time elements with m sample time points (per DQM time element). The total number of sample time points and the average time step can be obtained as [75-79]:

$$M_{\text{tot}} = n_T(m-1) + 1, \tag{71}$$

$$\Delta t = T/(M_{\text{tot}} - 1) = T/(n_T(m-1)), \tag{72}$$

where T is the length of the time span. Figure 1 presents the variations of $g'(t)$, with respect to t, for different values of n_T and m. It can be seen that the DQM solutions converge rapidly by increasing n_T and/or m. It is clear that by increasing the number of time elements, a smaller number of sampling time points is required to achieve accurate solutions. Note that the DQM solution results at m time points are utilized to obtain the solutions at all the time domains via the Lagrange interpolation scheme. Thus, we are able to find a continuous representation for function $g'(t)$ using the Lagrange interpolation scheme.

It is interesting to note that the DQM yields converged and rather accurate solutions using only $m = 3$ time points. From Figure 1, it can also be seen that as t increases, $g'(t)$ approaches a constant value. This constant value is actually the magnitude of L. Note that in cases shown in Figure 1, the value of t is in the range $0 \leq t \leq 7.5$. It is clear that in order to determine the magnitude of $L(= g'(\infty))$, it is not necessary to solve the initial-value problem (58) in all the time domains, $0 \leq t \leq \infty$. For instance,

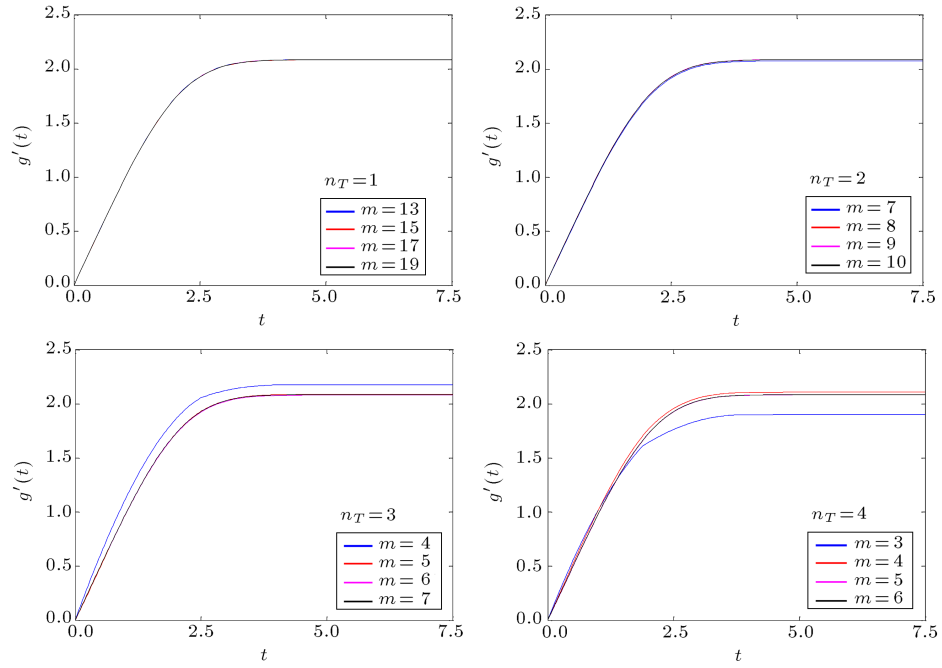

Figure 1. Convergence of DQM solutions with respect to the number of sample time points, m, and number of time elements, n_T.

Table 21. Convergence of solutions for $L = g'(t_\infty)$ ($n_T = 100$).

m	$t_\infty = 4.5$	$t_\infty = 5.5$	$t_\infty = 7.0$	$t_\infty = 8.0$	$t_\infty = 9.0$	$t_\infty = 9.25$	$t_\infty = 9.75$	$t_\infty = 10.0$
3	2.085	2.0854	2.0854	2.0854	2.0853	2.0853	2.0853	2.0853
4	2.085	2.0854	2.08541	2.08541	2.08541	2.08541	2.08541	2.08541
5	2.085	2.0854	2.08540917	2.08540917	2.08540917	2.08540917	2.08540917	2.08540917
6	2.085	2.0854	2.08540917	2.0854091764	2.0854091764	2.0854091764	2.0854091764	2.0854091764
7	2.085	2.0854	2.08540917	2.0854091764	2.085409176438	2.085409176438	2.085409176438	2.085409176438

as seen from Figure 1, one can solve the problem at the interval $0 \leq t \leq 7.5$ to find an approximation for L. In general, one can solve the problem in the time interval $0 \leq t \leq t_\infty$, where the magnitude of t_∞ depends on the desired level of convergence and accuracy. This can be clearly seen from the results shown in Table 21. These results are obtained using $n_T = 100$ and different values of m. From Table 21, one also sees that the accuracy of solutions for L will be improved by increasing the magnitude of t_∞. The best results with shown tolerance values can be achieved when $t_\infty = 9$. On the other hand, from Table 21, one sees that the DQM cannot produce highly accurate solutions when the number of sampling points is too small.

The convergence of solutions for $L = g'(9)$ is studied in Table 22. It can be seen that the DQM results converge quickly without instability for an increase in n_T and m. It can also be observed that by increasing the number of sample time points (i.e., m), a smaller number of time elements (i.e., n_T) are required to obtain solutions with identical accuracies. Besides, when m is too small, the rate of convergence is too slow and very large values of n_T are required to achieve accurate solutions. In other words, the rate of convergence of the solutions is more sensitive to m than to n_T. Thus, to obtain accurate solutions with a reasonable time step size, one should first choose the correct value of m and then increase n_T to reach the required level of accuracy. From Table 22, it is also observed that the magnitude of L is found to be converged up to 13 significant figures for a small grid size of $m = 8$.

In Table 23, the DQM solutions are compared with those of the Runge-Kutta scheme for fixed time step sizes. By comparing the DQM results with those of the Runge-Kutta scheme, one can conclude that the DQM can produce much better accuracy than the Runge-Kutta scheme using larger time step sizes. This illustrates the superiority of the DQM time

Table 22. Convergence of solutions for $L = g'(9)$.

m	$n_T = 5$	$n_T = 10$	$n_T = 15$	$n_T = 20$	$n_T = 25$	$n_T = 30$
6	2.085385346564	2.085405436352	2.085408770267	2.085409090448	2.085409150269	2.085409166448
7	2.085509533172	2.085409508201	2.085409206551	2.085409181810	2.085409177842	2.085409176906
8	2.085400798745	2.085409178934	2.085409176482	2.085409176438[a]	2.085409176437	2.085409176438
9	2.085406119885	2.085409175764	2.085409176418	2.085409176436	2.085409176438	2.085409176438
10	2.085409540756	2.085409176502	2.085409176440	2.085409176438	2.085409176438	2.085409176438
11	2.085409242435	2.085409176441	2.085409176438[b]	2.085409176438	2.085409176438	2.085409176438
12	2.085409167931	2.085409176438[c]	2.085409176438	2.085409176438	2.085409176438	2.085409176438
15	2.085409176444	2.085409176438	2.085409176438	2.085409176438	2.085409176438	2.085409176438
17	2.085409176438[d]	2.085409176438	2.085409176438	2.085409176438	2.085409176438	2.085409176438

[a]: $\Delta t = 0.0642857$; [b]: $\Delta t = 0.06$; [c]: $\Delta t = 0.081818$; [d]: $\Delta t = 0.1125$.

Table 23. Comparison of DQM solutions for $L = g'(9)$ with those of Runge-Kutta scheme for a fixed time step size.

Method	$\Delta t = 0.1125$	$\Delta t = 0.081818$	$\Delta t = 0.0642857$	$\Delta t = 0.06$	$\Delta t = 0.003$
Present	2.085409176438	2.085409176438	2.085409176438	2.085409176438	2.085409176438
Runge-Kutta	2.085408947590	2.085409109185	2.085409150100	2.085409156321	2.085409176438

Table 24. Convergence of solutions for the wall shear stress $f''(0) = \alpha$ for the Blasius equation ($n_T = 1$).

$m = 2$	$m = 3$	$m = 4$	$m = 5$	$m = 6$	$m = 7$
0.3320573362152	0.3320573362152	0.3320573362152	0.3320573362152	0.3320573362152	0.3320573362152

integration method over the classical Runge-Kutta scheme.

Now, using the value of $L = g'(\infty) \cong g'(9)$, we are able to solve Eq. (60) with the boundary conditions given in Eq. (61). Note that Eq. (60) can be solved in any arbitrary domain of interest. Since we are interested in determining the wall shear stress, $f''(0) = \alpha$, for the Blasius equation by the proposed method, we solved Eq. (60) in the interval $[0, 0.1]$. Table 24 demonstrates the convergence of solutions with respect to the number of sampling points. Only one DQM time element is used. An excellent convergence rate can be observed. It is interesting to note that the DQM can yield highly accurate solutions for the present problem using only $m = 2$ time points. Note that $m = 2$ is the smallest number of sample time points that can be used in the DQM for the solution of the present problem. The reason for this is that the present problem is a third-order nonlinear differential equation and has three initial conditions at the initial time point.

7. Conclusion

In this paper, a general formulation based on the DQM is proposed for solving general boundary layer problems. At first, a general formulation is presented for solving Blasius, Sakiadis, Falkner-Skan, MHD Falkner-Skan and Jeffery-Hamel boundary layer problems. An iterative DQM is also presented for solving unsteady, two-dimensional and three-dimensional, boundary layer problems. Finally, a simple scheme is proposed for solving the Blasius boundary layer equation. The efficiency, accuracy and convergence of the proposed formulation for solving general boundary layer problems are investigated and analyzed. It is shown that the proposed iterative DQM can predict the behavior of the general boundary layer accurately.

References

1. Schiliching, H., *Boundary Layer Theory*, 8th Ed., McGraw-Hill Inc (2004).
2. Howarth, L. "On the solution of the laminar boundary layer equations", *Proc. Royal Soc. London*, **164**, pp. 547-579 (1938).
3. Asaithambi, A. "Solution of the Falkner-Skan equation by recursive evaluation of Taylor coefficients", *J. Comput. Appl. Math.*, **176**, pp. 203-214 (2005).
4. Liao, S.J. "A kind of approximate solution technique which does not depend upon small parameters, Part 2: an application in fluid mechanics", *Int. J. Non-Linear Mech.*, **32**(5), pp. 815-822 (1997).
5. Liao, S.J. "An explicit, totally analytic solution of laminar viscous flow over a semi-infinite flat plate", *Commun. Nonlinear Sci. Numer. Simulat.*, **3**(2), pp. 53-57 (1998).

6. Liao, S.J. "A uniformly valid analytic solution of two dimensional viscous flow over a semi-infinite flat plate", *J. Fluid Mech.*, **385**, pp. 101-128 (1999).
7. He, J. "A new approach to nonlinear partial differential equations", *Commun. Nonlinear Sci. Numer. Simulat.*, **2**(4), pp. 230-235 (1997).
8. He, J. "Approximate analytical solution of Blasius equation", *Commun. Nonlinear Sci. Numer. Simulat.*, **4**(1), pp. 75-78 (1999).
9. Allan, F.M. and Syam, M.I. "On the analytic solutions of the nonhomogeneous Blasius problem", *J. Comput. Appl. Math.*, **182**, pp. 362-371 (2005).
10. Wang, L. "A new algorithm for solving classical Blasius equation", *Appl. Math. Comput.*, **157**, pp. 1-9 (2004).
11. Abbasbandy, S. "A numerical solution of Blasius equation by Adomian's decomposition method and comparison with homotopy perturbation method", *Chaos Solit. Fract.*, **31**, pp. 257-260 (2007).
12. He, J.H. "A simple perturbation approach to Blasius equation", *Appl. Math. Comput.*, **140**, pp. 217-222 (2003).
13. He, J.H. "Comparison of homotopy perturbation method and homotopy analysis method", *Appl. Math. Comput.*, **156**, pp. 527-539 (2004).
14. Kuo, B-L. "Thermal boundary-layer problems in a semi-infinite flat plate by the differential transformation method", *Appl. Math. Comput.*, **150**, pp. 303-320 (2004).
15. Fang, T., Guo, F. and Lee, C.F. "A note on the extended Blasius problem", *Appl. Math. Lett.*, **19**, pp. 613-617 (2006).
16. Cortell, R. "Numerical solution of the classical Blasius flat-plate problem", *Appl. Math. Comput.*, **170**, pp. 706-710 (2005).
17. Ahmad, F. "Degeneracy in the Blasius problem", *Electronic J. Diff. Eq.*, **92**, pp. 1-8 (2007).
18. Parand, K. and Taghavi, A. "Rational scaled generalized Laguerre function collocation method for solving the Blasius equation", *J. Comput. Appl. Math.*, **233**(4), pp. 980-989 (2009).
19. Ahmad, F. and Al-Barakati, W.H. "An approximate analytic solution of the Blasius problem", *Commun. Nonlinear Sci. Numer. Simulat.*, **14**, pp. 1021-1024 (2009).
20. Parand, K., Dehghan, M. and Pirkhedri, A. "Sinc-collocation method for solving the Blasius equation", *Phys. Lett. A*, **373**(44), pp. 4060-4065 (2009).
21. Cebeci, T. and Keller, H.B. "Shooting and parallel shooting methods for solving the Falkner-Skan boundary-layer equation", *J. Comput. Phys.*, **7**, pp. 289-300 (1971).
22. Asaithambi, N.S. "A numerical method for the solution of the Falkner-Skan equation", *Appl. Math. Comput.*, **81**, pp. 259-264 (1997).
23. Zhang, J. and Chen, B. "An iterative method for solving the Falkner-Skan equation", *Appl. Math. Comput.*, **210**, pp. 215-222 (2009).
24. Mastro, R.A. and Voss, D.A.R.A. "A quintic spline collocation procedure for solving the Falkner-Skan boundary-layer equation", *Comput. Methods Appl. Mech. Engrg.*, **25**, pp. 129-148 (1981).
25. Asaithambi, A. "A finite-difference method for the Falkner-Skan equation", *Appl. Math. Comput.*, **92**, pp. 135-141 (1998).
26. Asaithambi, A. "A second-order finite-difference method for the Falkner-Skan equation", *Appl. Math. Comput.*, **156**, pp. 779-786 (2004).
27. Asaithambi, A. "Numerical solution of the Falkner-Skan equation using piecewise linear functions", *Appl. Math. Comput.*, **159**, pp. 267-273 (2004).
28. Elgazery, N.S. " Numerical solution for the Falkner-Skan equation", *Chaos Solit. Fract.*, **35**, pp. 738-746 (2008).
29. Alizadeh, E., Farhadi, M., Sedighi, K., Ebrahimi-Kebria, H.R. and Ghafourian, A. "Solution of the Falkner-Skan equation for wedge by adomian decomposition method", *Commun. Nonlinear Sci. Numer. Simulat.*, **14**, pp. 724-733 (2009).
30. Yao, B. and Chen, J. "Series solution to the Falkner-Skan equation with stretching boundary", *Appl. Math. Comput.*, **208**, pp. 156-164 (2009).
31. Allan, F.M. and Al Mdallal, Q. "Series solutions of the modied Falkner-Skan equation", *Int. J. Open Problems Compt. Math.*, **4**(2), pp. 189-198 (2011).
32. Zhu, S., Wu, Q. and Cheng, X. " Numerical solution of the Falkner-Skan equation based on quasilinearization", *Appl. Math. Comput.*, **215**, pp. 2472-2485 (2009).
33. Rosales-Vera, M. and Valencia, A. "Solutions of Falkner-Skan equation with heat transfer by Fourier series", *Int. Commun. Heat Mass Transfer*, **37**, pp. 761-765 (2010)
34. Parand, K., Pakniat, N. and Delafkar, Z. " Numerical solution of the Falkner-Skan equation with stretching boundary by collocation method", *Int. J. Nonlinear Sci.*, **11**(3), pp. 275-283 (2011).
35. Abbasbandy, S. and Hayat, T. "Solution of the MHD Falkner-Skan flow by homotopy analysis method", *Commun. Nonlinear Sci. Numer. Simulat.*, **14**, pp. 3591-3598 (2009).
36. Yih, K.A. "MHD forced convection flow adjacent to a non-isothermal wedge", *Int. Commun. Heat Mass Transfer*, **26**(6), pp. 819-27 (1999).
37. Ishak, A., Nazar R. and Pop, I. "MHD boundary-layer flow of a micropolar fluid past a wedge with constant wall heat flux", *Commun. Nonlinear Sci. Numer. Simulat.*, **14**, pp. 109-118 (2009).
38. Abbasbandy, S. and Hayat, T. "Solution of the MHD Falkner-Skan flow by Hankel-Padé method", *Phys. Lett. A*, **373**, pp. 731-734 (2009).

39. Parand, K., Rezaei, A.R. and Ghaderi, S.M. "An approximate solution of the MHD Falkner-Skan flow by Hermite functions pseudospectral method", *Commun. Nonlinear Sci. Numer. Simulat.*, **16**, pp. 274-283 (2011).

40. Sakiadis, B.C. "Boundary-layer behaviour on continuous solid surfaces; boundary-layer equations for 2-dimensional and axisymmetric flow", *AIChE J.*, **7**, pp. 26-28 (1961).

41. Tsou, F.K., Sparrow, E.M. and Goldstein, R.J. "Flow and heat transfer in the boundary layer on a continuous moving surface", *Int. J. Heat Mass Transfer*, **10**, pp. 219-235 (1967).

42. Magyari, E. "The moving plate thermometer", *Int. J. Thermal Sci.*, **47**, pp. 1436-1441 (2008).

43. El-Arabawy, H.A.M. "Exact solutions of mass transfer over a stretching surface with chemical reaction and suction/injection", *J. Math. Statistics*, **5**(3), pp. 159-166 (2009).

44. Cortell, R. "Radiation effects for the Blasius and Sakiadis flows with a convective surface boundary condition", *Appl. Math. Comput.*, **206**(2), pp. 832-840 (2008).

45. Bataller, R.C. " Numerical comparisons of Blasius and Sakiadis flows", *Matematika*, **26**(2), pp. 187-196 (2010).

46. Ishak, A., Nazar, R. and Pop, I. "Boundary layer on a moving wall with suction and injection", *Chin. Phys. Lett.*, **24**(8), pp. 2274-2276 (2007).

47. Fang, T. "A note on the unsteady boundary layers over a flat plate", *Int. J. Non-Linear Mech.*, **43**, pp. 1007-1011 (2008).

48. Cortell, R. "Radiation effects in the Blasius flow", *Appl. Math. Comput.*, **198**, pp. 333-338 (2008).

49. Cortell, R. "Flow and heat transfer in a moving fluid over a moving flat surface", *Theor. Fluid Dyn.*, **21**, pp. 435-446 (2007).

50. Ishak, A., Nazar, N. and Pop, I. "The effects of transpiration on the flow and heat transfer over a moving permeable surface in a parallel stream", *Chem. Eng. J.*, **148**, pp. 63-67 (2009).

51. Liao, S. "A new branch of solutions of boundary-layer flows over an impermeable stretched plate", *Int. J. Heat Mass Transfer*, **48**, pp. 2529-2539 (2005).

52. Liao, S. "A new branch of solutions of boundary-layer flows over a permeable stretching plate", *Int. J. Non-Linear Mech.*, **42**, pp. 819-830 (2007).

53. Rashidi, M.M. "The modified differential transform method for solving MHD boundary-layer equations", *Comput. Phys. Commun.*, **180**, pp. 2210-2217 (2009).

54. Bognár, G. "Analytic solutions to the boundary layer problem over a stretching wall", *Comput. Math. Appl.*, **61**, pp. 2256-2261 (2011).

55. Fathizadeh, M., Madani, M., Khan, Y., Faraz, N., Yıldırım, A. and Tutkun, S. "An effective modification of the homotopy perturbation method for MHD viscous flow over a stretching sheet", *J. King Saud Univ. - Sci.* (2011), doi:10.1016/j.jksus.2011.08. 003

56. Wang, C.Y. "The three-dimensional flow due to a stretching flat surface", *Phys. Fluids*, **27**, pp. 1915-1917 (1984).

57. Ariel, P.D. "Generalized three-dimensional flow due to a stretching sheet", *Z. Angew Math. Mech.*, **83**, pp. 844-852 (2003).

58. Mehmood, A. and Ali, A. "Analytical solution of generalized three-dimensional flow and heat transfer over a stretching plane wall", *Int. Comm. Heat Mass Transfer*, **33**, pp. 1243-1252 (2006).

59. Liao, S. "An analytic solution of unsteady boundary-layer flows caused by an impulsively stretching plate", *Commun. Nonlinear Sci. Numer. Simulat.*, **11**, pp. 326-339 (2006).

60. Xu, H., Liao, S-J. and Pop, I. "Series solutions of unsteady three-dimensional MHD flow and heat transfer in the boundary layer over an impulsively stretching plate", *Europ. J. Mech. B/Fluids*, **26**, pp. 15-27 (2007).

61. Kumari, M. and Nath, G. "Analytical solution of unsteady three-dimensional MHD boundary layer flow and heat transfer due to impulsively stretched plane surfac", *Commun. Nonlinear Sci. Numer. Simulat.*, **14**, pp. 3339-3350 (2009).

62. Jeffery, G. B. "The two-dimensional steady motion of a viscous fluid", *Phil. Mag.*, **6**, pp. 455-465 (1915).

63. Hamel, G. "Spiralförmige Bewgungen zäher Füssigkeiten", *Jahresber. Deutsch. Math. Verein.*, **25**, pp. 34-60 (1916).

64. Makinde, O.D. and Mhone, P.Y. " Hermite-Padé approximation approach to MHD Jeffery-Hamel flows", *Appl. Math. Comput.*, **181**, pp. 966-972 (2006).

65. Esmaili, Q., Ramiar, A., Alizadeh, E. and Ganji, D.D. "An approximation of the analytical solution of the Jeffery-Hamel flow by decomposition method", *Phys. Lett. A*, **372**, pp. 3434-3439 (2008).

66. Sheikholeslami, M., Ghanji, D.D., Ashorynejad, H.R. and Rokni, H.B. "Analytical investigation of Jeffery-Hamel flow with high magnetic field and nanoparticle by Adomian decomposition method", *Appl. Math. Mech. -Engl. Ed.*, **33**(1), pp. 25-36 (2012).

67. Ganji, Z.Z., Ganji, D.D. and Esmaeilpour, M. "Study on nonlinear Jeffery-Hamel flow by He's semi-analytical methods and comparison with numerical results", *Comput. Math. Appl.*, **58**, pp. 2107-2116 (2009).

68. Domairry, DR.G., Mohsenzadeh, A. and Famouri, M. "The application of homotopy analysis method to solve nonlinear differential equation governing Jeffery-Hamel flow", *Commun. Nonlinear Sci. Numer. Simulat.*, **14**, pp. 85-95 (2009).

69. Moghimi, S.M., Domairry, G., Soleimani, S., Ghasemi, E. and Bararnia, H. "Application of homotopy analysis

method to solve MHD Jeffery-Hamel flows in non-parallel walls", *Adv. Engrg. Soft.*, **42**, pp. 108-113 (2011).

70. Esmaeilpour, M. and Ganji, D.D. "Solution of the Jeffery-Hamel flow problem by optimal homotopy asymptotic method", *Comput. Math. Appl.*, **59**, pp. 3405-3411 (2010).
71. Joneidi, A.A., Domairry, G. and Babaelahi, M. "Three analytical methods applied to Jeffery-Hamel flow", *Commun. Nonlinear Sci. Numer. Simulat.*, **15**, pp. 3423-3434 (2010).
72. Bellman, R.E. and Casti, J. "Differential quadrature and long term integrations", *J. Math. Analy. Appl.*, **34**, pp. 235-238 (1971).
73. Shu, C., *Differential Quadrature and Its Application in Engineering*, Springer, New York (2000).
74. Bert, C.W. and Malik, M. "Differential quadrature method in computational mechanics: A review", *ASME, Appl. Mech. Rev.*, **49**, pp. 1-28 (1996).
75. Eftekhari, S.A., Farid, M. and Khani, M. "Dynamic analysis of laminated composite coated beams carrying multiple accelerating oscillators using a coupled finite element-differential quadrature method", *ASME, J. Appl. Mech.*, **76**(6), 061001 (2009).
76. Eftekhari, S.A. and Khani, M. "A coupled finite element-differential quadrature element method and its accuracy for moving load problem", *Appl. Math. Model.*, **34**, pp. 228-237 (2010).
77. Khalili, S.M.R., Jafari, A.A. and Eftekhari, S.A. "A mixed Ritz-DQ method for forced vibration of functionally graded beams carrying moving loads", *Compos. Struct.*, **92**(10), pp. 2497-2511 (2010).
78. Jafari, A.A. and Eftekhari, S.A. "A new mixed finite element-differential quadrature formulation for forced vibration of beams carrying moving loads", *ASME, J. Appl. Mech.*, **78**(1), 011020 (2011).
79. Eftekhari, S.A. and Jafari, A.A. "Coupling Ritz method and triangular quadrature rule for moving mass problem", *ASME J. Appl. Mech.*, **79**(2), 021018 (2012).
80. Eftekhari, S.A. and Jafari, A.A. "Numerical simulation of chaotic dynamical systems by the method of differential quadrature", *Sci. Iran. B*, **19**(5), pp. 1299-1315 (2012)
81. Jafari, A.A. and Eftekhari, S.A. "An efficient mixed methodology for free vibration and buckling analysis of orthotropic rectangular plates", *Appl. Math. Comput.*, **218**, pp. 2672-2694 (2011)
82. Eftekhari, S.A. and Jafari, A.A. "A mixed method for free and forced vibration of rectangular plates", *Appl. Math. Model.*, **36**, pp. 2814-2831 (2012).
83. Eftekhari, S.A. and Jafari, A.A. "Vibration of an initially stressed rectangular plate due to an accelerated traveling mass", *Sci. Iran. A*, **19**(5), pp. 1195-1213 (2012)
84. Eftekhari, S.A. and Jafari, A.A. "Mixed finite element and differential quadrature method for free and forced vibration and buckling analysis of rectangular plates", *Appl. Math. Mech. Engl. Ed.*, **33**(1), pp. 81-98 (2012).
85. Liu, G.R. and Wu, T.Y. "An application of the generalized differential quadrature rule in Blasius and Onsager equations", *Int. J. Numer. Methods Engrg.*, **52**, pp. 1013-1027 (2001).
86. Girgin, Z. "Solution of the Blasius and Sakiadis equation by generalized iterative differential quadrature method", *Int. J. Numer. Methods Biomed. Engrg.*, **27**(8), pp. 1225-1234 (2011).
87. Na, T.Y., *Computational Methods in Engineering Boundary Value Problems*, Academic Press, New York (1979).
88. Salama, A.A. "Higher order method for solving free boundary problems", *Numer. Heat Transfer Pt. B: Fundam.*, **45**, pp. 385-394 (2004).
89. Fazio, R. "A novel approach to the numerical solution of boundary value problems on infinite intervals", *SIAM J. Numer. Anal.*, **33**, pp. 1473-1483 (1996).
90. Ariel, P.D. "Generalized three-dimensional flow due to a stretching sheet", *Z. Angew. Math. Mech.*, **83**, pp. 844-52 (2003).

Appendix A. Derivation of boundary layer equations

A.1 Blasius boundary layer equation

Assuming that the flow in the laminar boundary layer is two-dimensional, the continuity equation and the momentum equation may be expressed as:

$$u_{,x} + v_{,y} = 0, \tag{A.1}$$

$$uu_{,x} + vu_{,y} = \mu u_{,yy}, \tag{A.2}$$

where u and v are the velocity components in x and y directions of the fluid, respectively, and μ is the viscosity of the fluid. The boundary conditions for the velocity field are;

$$u = v = 0, \qquad \text{at} \qquad y = 0, \tag{A.3}$$

$$u = U_\infty, \qquad \text{at} \qquad x = 0, \qquad \text{and} \qquad y = \infty, \tag{A.4}$$

where U_∞ is the free stream velocity. A stream function, $\psi(x, y)$, is introduced, such that:

$$u = \psi_{,y}, \qquad v = -\psi_{,x}. \tag{A.5}$$

Note that the stream function satisfies the continuity equation (Eq. (A.1)). Substituting Eq. (A.5) into Eq. (A.2) gives:

$$\psi_{,y}\psi_{,xy} - \psi_{,x}\psi_{,yy} = \mu\psi_{,yyy}. \tag{A.6}$$

Introducing the following transformations [1];

$$f(\eta) = \frac{\psi}{\sqrt{U_\infty \mu x}}, \qquad \eta = y\sqrt{\frac{U_\infty}{\mu x}}, \tag{A.7}$$

one can obtain the Blasius boundary layer equation and the transformed boundary conditions given in Eqs. (1) and (2).

A.2 Falkner-Skan boundary layer equation

For Falkner-Skan boundary layer flow, the momentum equation is [1]:

$$uu_{,x} + vu_{,y} = \mu u_{,yy} + U_\infty U_{\infty,x}. \tag{A.8}$$

When the free stream velocity is of the form, $U_\infty = Kx^m$, where K and m are constants, it is possible to define the following similarity transformations:

$$f(\eta) = \sqrt{\frac{m+1}{2}}\frac{\psi}{\sqrt{U_\infty \mu x}},$$

$$\eta = y\sqrt{\frac{m+1}{2}}\sqrt{\frac{U_\infty}{\mu x}}, \tag{A.9}$$

which leads to the Falkner-Skan boundary layer equation given in Eq. (3), with $\beta_0 = 1$ and $\beta = \frac{2m}{m+1}$.

A.3 MHD Falkner-Skan boundary layer equation

The momentum equation for MHD Falkner-Skan boundary layer flow is:

$$uu_{,x} + vu_{,y} = \mu u_{,yy} + U_\infty U_{\infty,x} - \frac{\sigma B^2}{\rho_f}(u - U_\infty), \tag{A.10}$$

where σ is the electrical conductivity of the fluid, B is the magnetic field and ρ_f is the fluid density. Moreover, stream velocity and magnetic field are of the following forms [1]:

$$U_\infty = Kx^m, \qquad B = B_0 x^{(m-1)/2}. \tag{A.11}$$

Now, introducing the transformations given in Eq. (A.9) to Eq. (A.10) yields the MHD Falkner-Skan boundary layer equation given in Eq. (4), with $\beta = \frac{2m}{m+1}$ and $M^2 = \frac{2\sigma B_0^2}{\rho_f K(m+1)}$.

A.4 Sakiadis boundary layer equation

The governing differential equations (i.e., continuity and momentum equations) for the Sakiadis boundary layer flow are the same as those for the Blasius boundary layer flow (see Eqs. (A.1) and (A.2)). Assuming that the flat plate is stretched, with velocity $= U_w$, the boundary conditions for the Sakiadis boundary layer flow are [40]:

$$u = U_w, \qquad v = 0, \qquad \text{at} \qquad y = 0, \tag{A.12}$$

$$u = 0, \qquad \text{at} \qquad y = \infty. \tag{A.13}$$

Using transformations, $f(\eta) = \frac{\psi}{\sqrt{U_w \mu x}}$ and $\eta = y\sqrt{\frac{U_w}{\mu x}}$, one can obtain the transformed boundary conditions given in Eq. (5).

A.5 Unsteady two dimensional boundary layer equation

For an unsteady boundary layer developed by an impulsively stretching plate in a constant pressure viscous flow, the momentum equation is [59]:

$$u_{,t} + uu_{,x} + vu_{,y} = \mu u_{,yy}, \tag{A.14}$$

where t denotes the time. The boundary conditions and initial conditions for the velocity field are:

$$u = ax, \qquad v = 0, \qquad \text{at} \qquad y = 0, \tag{A.15}$$

$$u = 0, \qquad \text{at} \qquad y = \infty, \tag{A.16}$$

$$u = v = 0, \qquad \text{at} \qquad t = 0, \tag{A.17}$$

where a is a constant. Using the following similarity transformations;

$$f(\eta, \xi) = \frac{\psi}{x\sqrt{a\mu\xi}}, \qquad \eta = y\sqrt{\frac{a}{\mu\xi}},$$

$$\xi = 1 - \exp(-\tau), \qquad \tau = at, \tag{A.18}$$

one can derive the governing non-dimensional differential equation of the unsteady two dimensional boundary layer flow given in Eq. (6).

A.6 Unsteady three dimensional boundary layer equation

Consider the unsteady, three-dimensional laminar flow of an electrically conducting fluid caused by an impulsive stretching flat surface in two lateral directions in an otherwise quiescent fluid in the presence of a transverse magnetic field. It is assumed that, at time $t = 0$, the flat plate is stretched, with the velocity $u_w = ax$ and $v_w = by$, and its surface temperature is raised from T_∞ to the constant value, T_w. Under these conditions, the governing equations for the unsteady boundary layer flow and heat transfer for this problem are [60,61]:

$$u_{,x} + v_{,y} + w_{,z} = 0, \tag{A.19}$$

$$u_{,t} + uu_{,x} + vu_{,y} + wu_{,z} = \mu u_{,zz} - \frac{\sigma B^2}{\rho_f}u, \tag{A.20}$$

$$v_{,t} + uv_{,x} + vv_{,y} + wv_{,z} = \mu v_{,zz} - \frac{\sigma B^2}{\rho_f}v, \tag{A.21}$$

$$T_{,t} + uT_{,x} + vT_{,y} + wT_{,z} = \alpha T_{,zz}, \tag{A.22}$$

where w is the velocity component in the z-direction and α is the thermal diffusivity of the fluid. Other parameters and variables are defined in Sections A.1-A.4. The corresponding initial and boundary conditions are:

$$u = ax, \qquad v = by, \qquad w = 0,$$

$$T = T_w, \qquad \text{at} \qquad z = 0, \tag{A.23}$$

$$u = v = T = 0, \qquad \text{at} \qquad z = \infty, \tag{A.24}$$

where a and b are positive constants. Introducing the following similarity transformations:

$$\eta = z\sqrt{\frac{a}{\mu\xi}},$$

$$\xi = 1 - \exp(-\tau), \qquad \tau = at, \tag{A.25}$$

$$u = ax\frac{\partial f}{\partial \eta},$$

$$v = by\frac{\partial s}{\partial \eta},$$

$$w = -\sqrt{a\mu\xi}(f + s),$$

$$g = \frac{T - T_\infty}{T_w - T_\infty}, \tag{A.26}$$

one can derive the governing differential equations for unsteady three-dimensional flow given in Eqs. (8)-(10), subject to boundary conditions given in Eq. (11), where $c = b/a$ is a positive constant, $M = \sigma B^2/(\rho_f a)$ is the magnetic parameter and $\Pr = \mu/a$ is the Prandtl number.

A.7 Jeffery-Hamel boundary layer equation

Consider the steady unidirectional flow of an incompressible viscous fluid flow from a source or sink at the intersection between two rigid plane walls, where the angle between them is 2α. The continuity and momentum equations can be expressed in polar coordinates (r, θ) as [1]:

$$\frac{\rho_f}{r}\frac{\partial}{\partial r}(ru(r,\theta)) = 0, \tag{A.27}$$

$$u(r,\theta)\frac{\partial u(r,\theta)}{\partial r} = -\frac{1}{\rho_f}\frac{\partial p}{\partial r} + \mu\left[\frac{\partial^2 u(r,\theta)}{\partial r^2} + \frac{1}{r}\frac{\partial u(r,\theta)}{\partial r} + \frac{1}{r^2}\frac{\partial^2 u(r,\theta)}{\partial \theta^2} - \frac{u(r,\theta)}{r^2}\right] - \frac{\sigma B^2}{\rho_f r^2}u(r,\theta), \tag{A.28}$$

$$\frac{1}{\rho_f r}\frac{\partial p}{\partial \theta} - \frac{2\mu}{r^2}\frac{\partial u(r,\theta)}{\partial \theta} = 0, \tag{A.29}$$

where p is the fluid pressure and other parameters are defined in previous sections. It may be seen from Eq. (A27), that $ru(r,\theta) = f(\theta)$. Using dimensionless parameters;

$$f(\eta) = \frac{f(\theta)}{f(\theta)_{max}}, \qquad \eta = \frac{\theta}{\theta_{max}}, \qquad \theta_{max} = \alpha, \tag{A.30}$$

and eliminating P between Eqs. (A28) and (A29), one can obtain the Jeffery-Hamel boundary layer equation given in Eq. (12), where:

$$\mathrm{Re} = \frac{f(\theta)_{max}\theta_{max}}{\mu}, \qquad \mathrm{Ha} = \sqrt{\frac{\sigma B^2}{\rho_f \mu}}. \tag{A.31}$$

Biographies

Seyyed Aboozar Eftekhari received his BS degree in Mechanical Engineering from Sharif University of Technology, Tehran, Iran, in 2003. He then received his MS degree from Shiraz University, Iran, in 2006, and is currently a PhD degree student in the Department of Mechanical Engineering at K.N. Toosi University of Technology, Iran. His research interests include: applied mathematics, time integration schemes and vibration of continuous systems.

Ali Asghar Jafari received his PhD degree in Mechanical Engineering from the University of Wollongong, Australia, in 1994, and is currently Associate Professor in the Department of Mechanical Engineering at K.N. Toosi University of Technology, Iran. His research interests include: dynamics and vibrations of beams, plates and shells, composite structures and automotive engineering.